

**MICROSTRUCTURE AND PROPERTY EVOLUTION IN COLD WORKED  
EQUIATOMIC FE-PD DURING ISOTHERMAL ANNEALING**

by

Anirudha R. Deshpande

BE, University of Pune, 1999

Submitted to the Graduate Faculty of

School of Engineering in partial fulfillment

of the requirements for the degree of

Master of Science in Materials Science and Engineering

University of Pittsburgh

2004

UNIVERSITY OF PITTSBURGH  
SCHOOL OF ENGINEERING

This thesis was presented

by

Anirudha R. Deshpande

It was defended on

April 9, 2004

and approved by

John A. Barnard, Professor and Chair, Materials Science and Engineering

William A. Soffa, Professor, Materials Science and Engineering

Thesis advisor: Jörg M. K. Wiezorek, Assistant Professor, Materials Science and Engineering

**MICROSTRUCTURE AND PROPERTY EVOLUTION IN COLD WORKED  
EQUIATOMIC FE-PD DURING ISOTHERMAL ANNEALING**

Anirudha R. Deshpande, MS

University of Pittsburgh, 2004

In this work the evolution of microstructure and magnetic properties in cold deformed, equiatomic FePd during isothermal annealing has been studied. During annealing of the disordered cold deformed FePd at temperatures below the critical ordering temperature,  $T_c = 928$  K (655 °C), concomitant annealing and ordering (FCC  $\rightarrow$  L1<sub>0</sub>) reactions take place. The effects of the processing parameters - stored energy of cold work and temperature - on microstructural and property evolution are investigated. The combined solid state reaction (CR) produces complex microstructures that exhibit enhanced magnetic hardness (coercivity) relative to the conventionally processed material. The magnetic age hardening response of the CR processed FePd has been reported. For fully equiaxed polycrystalline microstructures of the ordered FePd phase a correlation between the average grain size and the coercivity has been observed. Based on these purely microstructural observations a qualitative coercivity mechanism analysis has been performed in order to elucidate the origin of the decrease in magnetic hardness (coercivity) in the overaged condition.

## TABLE OF CONTENTS

LIST OF TABLES .....	vii
LIST OF FIGURES.....	viii
PREFACE .....	xi
1.0 INTRODUCTION.....	1
1.1 THE $\gamma_1$ -FePd PHASE .....	1
1.2 RESEARCH OBJECTIVES .....	5
2.0 BACKGROUND .....	7
2.1 THE ORDERING PHASE TRANSFORMATION .....	7
2.2 ANNEALING PHENOMENON .....	9
2.2.1 The Deformed State .....	9
2.2.2 Annealing .....	10
2.3 COMBINED REACTION TRANSFORMATION .....	14
2.3.1 Introduction .....	14
2.3.2 Sequential and Simultaneous Combined Reactions .....	15
2.3.3 Combined Reactions in Equiatomic FePd Intermetallics .....	17
2.4 COLD WORKING .....	18
2.4.1 Cold Rolling .....	18
2.4.2 Equal Channel Angular Pressing .....	19

3.0 EXPERIMENTAL PROCEDURE.....	22
3.1 SAMPLE PREPARATION .....	22
3.1.1 Alloy Preparation .....	22
3.1.2 Heat Treatments .....	22
3.1.3 Homogenization and Disordering Annealing Treatment .....	23
3.2 COLD DEFORMATION .....	23
3.2.1 Cold Rolling .....	24
3.2.2 Equal channel angular pressing .....	24
3.3 ISOTHERMAL ORDER-ANNEALING .....	24
3.4 CHARACTERIZATION TECHNIQUES .....	25
3.4.1 X-ray diffraction .....	25
3.4.2 Electron Microscopy .....	25
3.4.3 Magnetic Measurements .....	26
3.4.4 Grain size analysis .....	26
4.0 RESULTS AND DISCUSSION .....	29
4.1 RECRYSTALLIZED DISORDERED STATE .....	29
4.2 ONE PASS ECAP – MICROSTRUCTURE AND PROPERTY EVOLUTION .....	30
4.2.1 Deformed microstructure .....	30
4.2.2 Magnetic properties.....	32
4.2.3 X-ray diffraction – Evolution of LRO .....	34
4.2.4 Microstructural Observations.....	36
4.2.5 Discussion .....	45
4.3 COLD ROLLED TO 97% REDUCTION IN THICKNESS – MICROSTRUCTURE AND PROPERTY EVOLUTION.....	49

4.3.1 Deformed microstructure .....	50
4.3.2 Magnetic properties .....	51
4.3.3 X-ray diffraction – Evolution of LRO.....	53
4.3.4 Microstructural Observations.....	56
4.3.5 Discussion .....	67
5.0 SUMMARY AND CONCLUSIONS .....	79
6.0 RECOMMENDATIONS FOR FUTURE WORK .....	82
BIBLIOGRAPHY.....	84

## LIST OF TABLES

Table-1 Comparison of intrinsic magnetic properties of FePd with other L1 <sub>0</sub> ferromagnets .....	3
Table-2 c/a ratios obtained for the condition of maximum coercivity at various annealing temperatures.....	55
Table-3 Some pertinent grain size measurements for the condition of peak coercivity and in the overaged condition.....	62

## LIST OF FIGURES

Figure – 1 Unit cell of tetragonal L1 <sub>0</sub> phase.....	1
Figure – 2 Relevant section for the binary Fe Pd phase diagram.....	2
Figure – 3 Polytwinned microstructural morphology.....	8
Figure-4 A TTT diagram for a process involving recrystallization and phase decomposition.....	16
Figure – 5 Schematic for the ECAP cold deformation process a) $\phi = 0$ , b) $\Psi > 0$ .....	19
Figure-6 The distribution of strain, as determined by a FEA model , a) One pass ECAP, b) Two pass ECAP, c) Three pass ECAP.....	21
Figure-7 a) BSE,SEM micrograph with grain boundaries delineated. b) Individual grains identified by the image analysis program and used for area determination.....	28
Figure – 8 BSE, SEM micrograph of disordered recrystallized Fe,Pd.....	29
Figure-9 a) BSE-SEM micrograph of disordered FePd in the deformed state after one pass ECAP. b) TEM bright field multi-beam micrograph of the dense dislocation cell structure in a grain in the FePd after ECAP, inset – SADP of the grain with a ZA of [100].....	31
Figure -10 hysteresis loop, corrected for the shape of the sample using the demagnetizing factor for an oblate spheroid.....	32
Figure-11 Coercivity evolution as a function of annealing time during order annealing after one pass ECAP.....	33
Figure -12 Evolution of the LRO parameter as a function of annealing time.....	35
Figure -13 Examples of SEM BSE micrographs of the microstructural evolution in the cold-deformed Fe-Pd during annealing at 500°C a) 3 hours, b) 5 hours, c) 12 hours, c) details of CR transformed grains that nucleate at transition bands between heavily deformed regions of significantly different orientation.....	37

Figure-14 SEM, BSE micrographs of the microstructures after a) 12 hours and b) 24 hours of annealing at 500°C.....	39
Figure – 15 Example TEM micrographs depicting the evolution of L10 – type LRO in the non-CR transformed region. a) Bright field, $g = 002$ , off [110], b) corresponding dark field with $g=001$ , both for 5 hours annealing at 500°C. Traces of dodecahedral planes parallel to [1-11] and [1-1-1] are marked in a). c) multibeam bright field, beam direction [001], inset SADP, for 24 hours of annealing at 500°C .....	42
Figure -16 Multi-beam bright field TEM micrograph depicting an example of new L1 <sub>0</sub> – ordered CRP grains, in the cold-deformed Fe-Pd after 10 hours of annealing at 500°C.....	44
Figure -17 BSE, SEM image of the microstructure in the cold rolled to 97% reduction in thickness sample.....	50
Figure -18 Coercivity evolution as a function of annealing time during order annealing after 97% reduction in thickness by cold rolling.....	52
Figure-19 Representative set of a symmetric ( $\theta$ -2 $\theta$ ) XRD scan obtained for cold rolled samples annealed at 600°C for a time period at which a maximum in coercivity is observed (3 hours).....	54
Figure -20 BSE, SEM micrograph showing a microstructural state that has been partially transformed by CR process.....	57
Figure-21 BSE, SEM images of the microstructure after annealing at 400°C a) at the peak in the magnetic age hardening curve – annealed for 7 days; b) in the overaged condition – annealed for 8 days.....	58
Figure-22 BSE, SEM images of the microstructure after annealing at 500°C a) at the peak in the magnetic age hardening curve – annealed for 6 hours, b) in the overaged condition – annealed for 10 hours.....	59
Figure-23 BSE, SEM images of the microstructure after annealing at 600°C a) at the peak in the magnetic age hardening curve – annealed for 3 hours, b) in the overaged condition – annealed for 8 hours.....	60
Figure-24 Grain size distribution for samples order annealed at 600°C. a) For the peak coercivity condition, b) in the overaged condition.....	63
Figure-25 a) Bright field, multibeam TEM micrograph, near [001] ZA (3h-600C) b) Selected area diffraction pattern, [001] ZA (3h-600°C).....	64
Figure-26 a) Bright field, multibeam TEM micrograph, near [001] ZA (8h-600C) and as inset a selected area diffraction pattern,[001] ZA, from a CR-transformed L10 FePd grain. b) Bright	

field TEM micrograph of CR-transformed grains showing twinning (8h-600C).....66

Figure-27 Comparison of previously reported [Greenberg] work on ordering kinetics with the experimental data obtained in this study.....70

## **PREFACE**

There are multiple people who deserve to be thanked for helping me with this endeavor. Firstly I would like to thank Dr. Wiezorek, for providing me with this wonderful opportunity to pursue my interest in this field. I would also like to thank the National Science Foundation for providing funding for this research program. The help provided by Dr. Huiping Xu with initial TEM and SEM experiments is greatly appreciated. I would also like to thank Cole van Ormer and Al Stuart for their help with various microcharacterization techniques. I would like to thank Dr. S. Saha for his help with the vibrating sample magnetometer work. The Pitt-MSE graduate students all provided invaluable help over years, especially A. Kulowits, M. Renavikar, who helped me with the initial experimental work. I thank them all. I would also like to express my gratitude to Dr Soffa, for he has been a great teacher and has helped me to develop a good theoretical base. I would also like to thank Dr J.R. Blachere for the time spent having extremely interesting discussions on the X-Ray Diffraction part of this work. Finally I thank Dr. Barnard for his encouragements and taking some time out of his busy schedule to be on my committee.

## 1.0 INTRODUCTION

### 1.1 THE $\gamma_1$ -FePd PHASE.

At room temperature FePd of equiatomic composition forms a stable tetragonal  $L1_0$  ordered intermetallic phase ( $\gamma_1$ ). The conventional unit cell of the  $L1_0$  phase that has a simple tetragonal Bravais lattice is as shown in figure – 1.

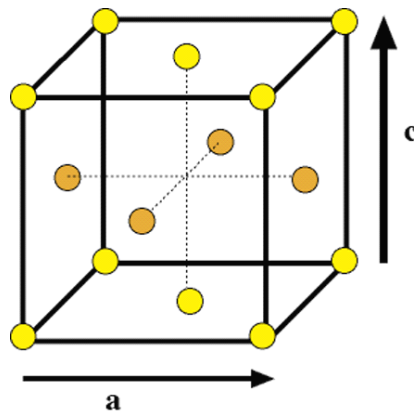


Figure – 1 Unit cell of tetragonal  $L1_0$  phase

The ordered FePd phase can be envisaged as a layered structure consisting of alternating stacking of pure Fe and pure Pd planes of the type (002). The relevant section of the phase diagram for this binary system is shown in figure-2. The use of the conventional unit cell shown in figure-1 clearly indicates the relationship to the cubic close-packed or face-centered cubic (FCC) parent

phase, the disordered  $\gamma$ -phase (Fe,Pd)-solid solution, which is stable at temperatures above  $T_c = 928 \text{ K}$  ( $655 \text{ }^\circ\text{C}$ ).

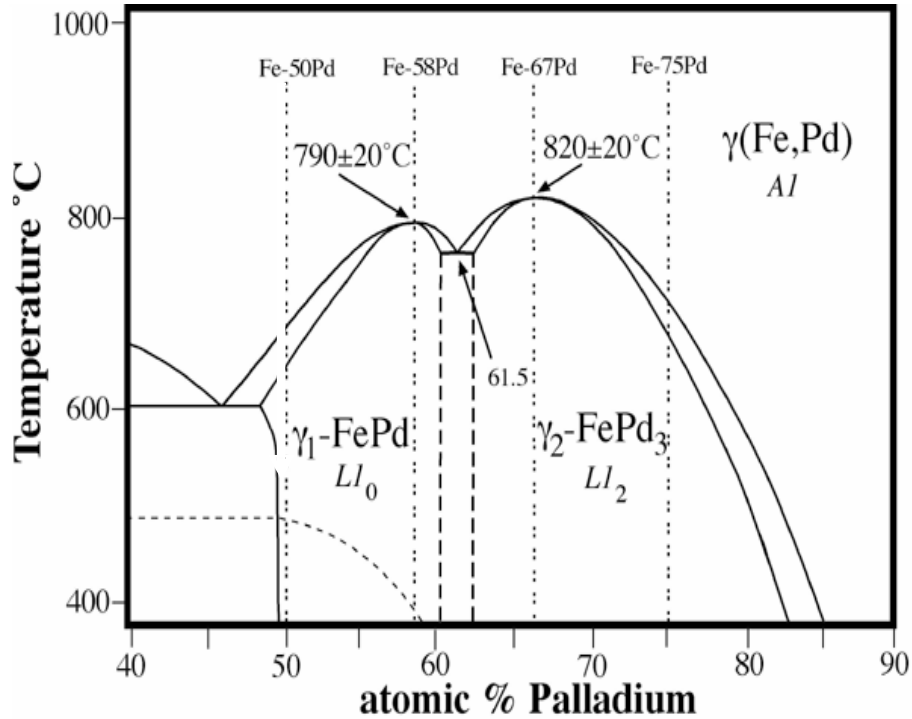


Figure – 2 Section of the binary Fe-Pd phase diagram.

$\gamma_1$  - FePd based alloys are an important member of the family of technologically interesting intermetallics, such as CoPt, FePt, TiAl, and MnAl, that can produce the  $L1_0$  phase at room temperature. The  $L1_0$  phase in the FePd alloys exhibits a high uniaxial magnetocrystalline anisotropy with an 'easy' magnetization axis parallel to  $[001]$ , a large theoretical B-H product and good corrosion and mechanical properties. This combination of properties renders FePd based  $L1_0$  intermetallics very attractive for a range of permanent magnet and thin film applications [1]. As can be seen from table-1 the intrinsic properties of the intermetallic  $\gamma_1$  phase are comparable

to those of rare earth magnets, However, the technical magnetic properties reported for conventionally processed FePd based alloys are disappointingly low [2,3]. This indicates that the technical properties of the FePd alloys are very sensitive to the microstructure.

Table-1 Comparison of intrinsic magnetic properties of FePd with other L1<sub>0</sub> ferromagnets [8]

	K <sub>1</sub> erg cm <sup>-3</sup> (x 10 <sup>7</sup> )	M <sub>s</sub> emu cm <sup>-3</sup>	H <sub>a</sub> kOe	T <sub>c</sub> K	δ nm	γ erg cm <sup>-2</sup>	D <sub>c</sub> nm	(BxH) <sub>max</sub> MGOe
FePd	1.8	1100	33	760	7.5	17	200	48
FePt	6.6	1140	116	750	3.9	32	340	51
CoPt	4.9	800	123	840	4.5	28	610	25
MnAl	1.7	560	69	650	7.7	16	710	12
Fe <sub>14</sub> Nd <sub>2</sub> B	4.6	1270	73	585	4.6	27	230	64
SmCo <sub>5</sub>	11-20	910	240-440	1000	2.2-3.0	42-57	710-960	33

Conventional processing involves the heating of these alloys to a temperature where the FCC phase is stable followed by rapid quenching to a low temperature to retain the FCC phase. The quenched material is then heat treated at a temperature in the L1<sub>0</sub> phase field. The thermal activation at this elevated temperature is capable to facilitate the phase transformation of metastable FCC → to stable L1<sub>0</sub>. Conventional processing of these alloys produces a hierarchy of microstructural entities, such as polytwins and antiphase boundaries (APBs), which strongly influence hard magnetic properties. It has been shown that the presence of a well-developed polytwin microstructure is detrimental to hard magnetic properties [4]. Thermomechanical processing routes have been successfully employed to eliminate the polytwinned microstructure [5]. These routes have been based on a **combined reaction (CR)** mode of microstructural

transformation, involving the interplay between ordering and annealing reactions, such as recovery and recrystallization. The scale and morphology of the products of the CR transformation are extremely important in determining the magnetic properties and can be altered by a judicious combination of the amount of cold work and the transformation temperature and time [5].

The driving force for the recrystallization reaction stems from the stored energy of cold work. Increasing the driving force for recrystallization at a given transformation temperature can have the effects of suppressing the polytwin structure and decreasing the length scale of the CR products [5]. An enhancement in the transformation kinetics in these CR processed samples relative to conventionally processed samples without prior cold-deformation has also been reported previously [5]. However, the details of the microstructural evolution during CR processing and correlation between the evolving microstructural morphology and scale with magnetic properties have not been developed sufficiently. Hence, further experimental study is required to establish a better understanding of the relationships between processing parameters, evolution of microstructure and the resulting properties for CR processed FePd alloys. This is attempted here using a model Fe-Pd alloy of equiatomic composition, cold-deformation by various methods, microstructural investigations by x-ray diffraction (XRD), scanning and transmission electron microscopy (SEM and TEM) and property measurements using M-H loops obtained with a vibrating sample magnetometer (VSM).

## 1.2 RESEARCH OBJECTIVES

Further optimization of magnetic properties of CR processed Fe-Pd may be possible by the appropriate combination of temperature of transformation and the amount of cold work. This study aims to explore a processing parameter matrix of annealing temperature, annealing time and amount of strain of cold work to achieve a further reduction in the microstructural length scale of the transformation products, while suppressing the formation of microstructural morphologies detrimental to the enhancement of magnetic properties.

Hence, in this study the stored energy of cold work, the driving force for recrystallization, imparted to the material has been altered by using different cold deformation techniques. Equal channel angular pressing (ECAP) and cold rolling have been utilized to achieve this effect. The evolution of microstructure has been investigated using techniques, such as SEM and TEM. The progression of the ordering process has been studied using XRD. VSM measurements have been used to obtain hysteresis loops of the thermomechanically processed material and the data gathered from these M-H loops has been used to study the evolution of the magnetic properties. Computer assisted image analysis has been used to obtain quantitative information about the microstructural changes using metrics such as the grain size and its distribution. The effect of these microstructural parameters on the observed coercivity has been studied.

Using this approach it was attempted to accomplish the following objectives during this study –

1. Identify a thermomechanical processing strategy that aids optimization of the hard magnetic properties, here taken as increase of the coercivity.
2. Develop a quantitative understanding of the effect of prior strain of cold-deformation on the kinetics and the nature of the FCC  $\rightarrow$  L1<sub>0</sub> phase transformation.

3. Develop a quantitative understanding of the evolution of the microstructure in terms of microstructural metrics, such as grain size, percentage transformed by non-conventional mode etc., during thermomechanical processing.
4. Develop a qualitative understanding of the effect of these microstructural metrics on the coercivity exhibited by the non-conventionally or CR processed samples.

## 2.0 BACKGROUND

This study is aimed at the development of an understanding of various elementary processes involved with the evolution of the microstructure and magnetic property in a model FePd system with equiatomic composition. Solid state processes, such as the ordering phase transformations, recovery, recrystallization and grain growth, occurring during annealing of the material in the cold worked state are being investigated. In this section these basic processes are briefly reviewed before subsequent reporting on their application to the FePd system.

### 2.1 THE ORDERING PHASE TRANSFORMATION

Conventional processing of the equiatomic Fe-Pd alloys involves thermally activated ordering of the disordered phase at temperatures below the critical ordering temperature without prior cold-deformation of the FCC phase. The conventional processing establishes the ordered  $L1_0$  phase of  $\gamma_1$ -FePd by one of two different routes. The first involves continuous cooling of the equiatomic Fe-Pd materials from the high temperature  $\gamma_1$ -phase field to room temperature at suitably slow rates. The second involves rapid quenching of the disordered solid solution FCC ( $\gamma$ ) (Fe, Pd) from  $T > T_c \approx 938$  K to room temperature followed by isothermal annealing at  $T < T_c$  to induce ordering from FCC to  $L1_0$  structure. The disorder-to-order transformation is thermodynamically a first-order type phase transformation with metastable FCC ( $\gamma$ )  $\rightarrow$  stable  $L1_0$  ( $\gamma_1$ ) transformation.

This ordering transformation involves the nucleation of coherent precipitates of  $\gamma_1$ -phase throughout the grains of the disordered  $\gamma$ -matrix. The process of atomic ordering results in the formation of the tetragonal lattice of the product phase. Any of the three  $\langle 010 \rangle$  axes of the cubic matrix may be altered in dimension to produce a tetragonal structure. Thus, in accordance with the three possible orientations of the c-axis of the tetragonal structure the precipitation reaction can generate three variants of the product phase in a given parent phase grain. This transformation is associated with a transformation strain. The transformation strains affect the transformation process, which results in structural self-organization. The resultant structure consists of regular plate-like misoriented crystallite-twins. Such crystallites may be referred to as c-domains. Adjacent c-domains in a polytwinned plate join together on invariant  $\{110\}_{\text{FCC}}$  planes. The tetragonal axes in the adjacent plates are misoriented through an angle of  $\sim 90^\circ$  [4,6,7]. The regular crystallite structure, having a twinned morphology with a dodecahedral  $\{110\}$  plane as the conjugate plane is referred to as the polytwinned structure and is depicted in Figure-3.

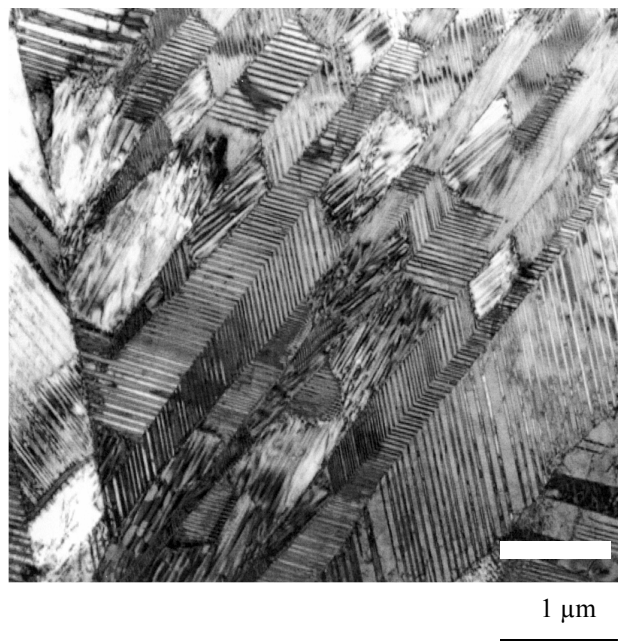


Figure – 3. Polytwinned microstructural morphology

Previous Studies [4,8] have ascribed the rather disappointing magnetic properties of these Fe-Pd alloys to the polytwinned structure that develops during the conventional processing. The c-axes in adjacent polytwin lamella are misoriented by about  $90^\circ$ . In the uniaxial ferromagnetic  $L1_0$  phase, the easy axis of magnetization lies along the c-axis. Therefore the polytwin interfaces also act as  $90^\circ$  magnetic domain walls. Magnetization reversal is most effectively accomplished by the motion of  $180^\circ$  Bloch walls. Such  $180^\circ$  walls 'zig-zag' across the polytwin interfaces between adjacent lamellae with differently oriented c-axes in a given polytwinned grain. The polytwin interfaces cannot effectively pin  $180^\circ$  domain walls, which results in easy magnetization reversal by the unhindered motion of  $180^\circ$  walls along the length of the polytwin lamellae. This effectively reduces the magnetic hardness in polycrystals with polytwinned morphology.

## **2.2 ANNEALING PHENOMENON**

### **2.2.1 The Deformed State**

According to previous studies the FCC-related FePd base intermetallics have been categorized as a low stacking fault energy (LSFE) material [9]. During the process of cold rolling of FCC metals with LSFE tend to undergo deformation by both dislocation glide and a twinning mode. Previous work concluded that disordered Fe-Pd also exhibits these characteristics [10,11,12]. The resultant deformation structures consist of a lamellar morphology, with the twinning plane,  $\{111\}$ , making angles of  $0^\circ$ - $30^\circ$  with the rolling plane. With additional deformation, rotation of the twinning plane towards the rolling plane occurs. At large deformations, shear, micro- and transition bands consisting of very fine, highly misoriented crystallites appear. These bands tend to make angles of  $25^\circ$ -  $40^\circ$  with the rolling plane and are seen to be spanning over many grains.

The dislocation density in the regions of these deformation bands is very high. As the driving force for recrystallization stems from the stored energy of cold work, which is associated with the dislocation structures, these regions with high defect density can act as preferred sites for nucleation of recrystallized grains.

With the exception of maintaining the cross sectional area, the process of deformation using equal channel angular pressing is similar to that in cold rolling. However with multiple passes, in principle, much larger amounts of energy of cold work can be stored in the material. Microstructural features such as shear bands, transition bands, deformation bands and arrays of stacking faults would be produced in this process. With large amounts of deformation (using multiple passes) structures consisting entirely of sub-grains or a so-called deformation cell structure with all of the above-mentioned defect configurations can be expected.

### **2.2.2 Annealing**

The three processes of recovery, recrystallization and grain growth together constitute the three distinguished annealing phenomena. Recovery refers to all those processes of defect rearrangements in the deformed microstructure, which do not involve the sweeping of the deformed structure by migrating high-angle grain boundaries. Thus, during recovery the deformed polycrystalline aggregate retains its identity, while the density of crystal defects (mostly dislocations and vacancies) and their distribution changes. Recovery has been associated with the decrease in number of line and point defects present in the deformed material. The annihilation of dislocations with opposite signs gliding on the same glide planes, thermally assisted climb of edge dislocations leading to polygonization, annihilation of excess vacancies

with grain boundaries and line defects acting as vacancy sinks are some of the mechanisms by which this process has been described previously [13].

The various mechanisms for recovery are facilitated by diffusion of vacancies under the influence of thermal activation. However, during annealing of disordered alloys at temperature lower than the critical ordering temperature some new concerns arise. The diffusion of a vacancy in a medium is governed by factors, such as the jump distance for the elementary diffusion process, thermal activation, the coordination number, and a correlation factor that takes into account the ability of the vacancy to 'hop' into a particular site [14]. During annealing at temperatures for which the ordered phase is stable, the elementary processes by which vacancy diffusion takes place and therefore recovery occurs are affected by the evolution of the degree of long range order. It is no longer likely for the vacancy to diffuse in any direction at random, as doing so would tend to disrupt the atomic order for certain directions. Consequently the correlation factor reduces from its maximum value of unity (the reduction being a function of the degree of long range order at that particular instance). The reduction in the correlation factor leads to a decrease in the diffusion coefficient for vacancies and therefore slows the kinetics of all the vacancy diffusion assisted processes in annealing. Hence, the chemical ordering is expected to have a strong effect on the details of the recovery processes in the ordering Fe-Pd model alloys studied here.

Recrystallization refers to the process by which stress free, equiaxed grains are produced from a heavily stressed microstructural state. This topic has been extensively studied for elemental metals and alloys and the theories of recrystallization have been debated extensively in the literature [15]. Central to all these theories has been the postulate that a stress free grain would be nucleated in the region of high deformation content. Previous studies [16,17,18,19] have

clarified that the mechanism of nucleation of a recrystallized grain is intimately linked with the structure of the deformed metal and specifically with the degree of heterogeneity of orientation within each deformed grain. In line with these observations some theories of recrystallization have been promulgated [20,21,22,23]. The main ideas in these theories include the following models or concepts:

- 1) A classical nucleation (or fluctuation) phenomenon involving a heterogeneous or homogeneous mode;
- 2) Local growth of a polygonized region in the deformed sub-structure to eventually produce a viable nucleus;
- 3) Coalescence of neighboring sub-grains by the annihilation of dislocations constituting the sub-boundaries between them;
- 4) Strain-induced boundary migration (SIBM) model, in which a sub-grain within a deformed region grows into its neighbor, forming a bulge which has the orientation of the source grain and is largely free of dislocations.

Of these four conceptual models that have been proposed, the classical nucleation theory has been discredited, as the driving force for recrystallization is not sufficient to account for the energy required to produce a high angle grain boundary. The last three theories involve the rearrangement of dislocation sub-structure (recovery) as a pre-requisite to produce viable high-angle boundaries and do not require the formation of a truly new orientation grain or nucleus in the cold-worked material. Rather, they are based on the further evolution of specific defected regions already present after deformation. Given the complexity involved in the analysis of the phenomenon of recrystallization, one or all theories in tandem can be sufficient to explain the experimental observations. However, the details are still discussed controversially [24].

Various kinetic models have been used to quantify the rate of the process of recrystallization [24,25]. The Johnson-Mehl-Avrami-Kolmogorov (JMAK) model seems to be the most popular model. This model expresses the volume fraction recrystallized as a function of time by the relation

$$X_v = 1 - \exp(-Bt^k) \quad \text{--} \quad (1)$$

Here, B and k are constants depending on the material and thermomechanical processing parameters (e.g. T,  $\epsilon_{cw}$ ).

The annealing phenomenon of recrystallization is complete once the new, essentially strain-free grains have grown sufficiently to impinge on one another. At this point the driving force for recrystallization has been expended.

If annealing is continued after recrystallization is essentially complete, grain growth entails as the dominant microstructure altering process. The driving force for grain growth arises from the reduction in excess surface energy associated with grain boundaries. The process of grain growth is affected by factors such as the impurity content at the grain boundaries, the orientation relationships across the grain boundaries, the defect content in front of a moving high angle grain boundary etc. Grain growth is a phenomenon facilitated by boundary diffusion. Thus, the nature (chemical order, atomic structure, morphology) of the GBs or interfaces plays a very important role in determining growth kinetics. Structurally and compositionally different segments of GBs exhibit different rates of mobility. This would manifest itself in the resultant three-dimensional grain structure that would be obtained during the process of grain growth. It is expected that the largest grains are bound by highly mobile interfaces and that smaller grains that have been unable to grow are bound by low mobility interfaces.

Processes of recovery usually lead to annihilation of excess defect content in the matrix grains. Thus, high local concentrations of strain energy, conducive to promote recrystallization can become scarce, therefore affecting recrystallization kinetics. Moreover the process of recovery can also affect growth, as it can alter both the impurity content and the defect content across a high angle grain boundary. Hence, it can be inferred that the elementary processes in annealing are not mutually exclusive, but rather they are interdependent or coupled and may occur simultaneously. The interplay between all these solid state reactions has to be considered which has made the theoretical modeling of annealing phenomenon quite complex.

## **2.3 COMBINED REACTION TRANSFORMATIONS**

### **2.3.1 Introduction**

Solid state reactions occur under the influence of thermodynamic driving forces. Reactions, such as recrystallization and diffusional phase transformations have a characteristic thermodynamic driving force associated with them. In many thermomechanically processed metallic alloy systems more than one driving force and more than one type of reaction are present, which can strongly affect the microstructural evolution during thermally activated processing [26]. Under such circumstances, it is always possible to have more than one reaction change the microstructural state of the system. Microstructural rearrangement or transformation facilitated by a process for which the overall driving force is a function of more than one possible elementary solid state reaction are referred to as combined reactions (CR) [27].

CRs are frequently encountered in the field of physical metallurgy. Typical examples are precipitation hardening in cold worked stainless steels and martensitic transformations in shape

memory alloys. Due to the interplay of the multiple driving forces for the different individual solid state reactions, the kinetics of these CR processes are altered from those of the individual reactions. Possible synergistic effects can exist amongst the various driving forces. Moreover, due to the different functional dependence of each process on thermal activation, there could be coordinates in temperature-time space for which one reaction could be favored as compared to another. Such scenarios can lead to simultaneous or sequential combined reactions. An important hallmark of a CR is the microstructure that develops as a result of the process. The microstructural development can provide insight regarding the possible mode of combined reaction (e.g. sequential vs. simultaneous) and also about the kinetics of the process. Therefore, here in this brief review a background will be developed for the investigation of the annealing phenomena for the FePd alloys studied here in light of the CR transformation mode.

### **2.3.2 Sequential and Simultaneous Combined Reactions**

The kinetics of a CR are governed by the tendency of a system to maximize the rate of dissipation of excess free energy. The kinetics of any solid state reaction would be a function of the driving force (for the individual reaction) and the mobility of atoms (in case of diffusion assisted transformations). Thus depending upon the relative magnitudes of both these parameters, either sequential reactions or simultaneous reactions can occur. Though useful, such quantitative estimates assume a mean field approximation, and therefore may not be able to entirely correctly predict the observed behavior. Nevertheless they do provide a background for a theoretical analysis of the possible reaction paths.

Experimentally derived time-temperature-transformation (TTT) diagrams provide a more accurate description of the system behavior. In temperature-time space, reaction kinetics can be appropriately depicted using a TTT diagram. These diagrams can help us identify the onset and completion of various reactions that are possible under the influence of appropriate thermodynamic driving forces. As an example, a TTT diagram for a process involving recrystallization (R in the figure) and decomposition (D in the figure) of a phase is shown in figure-4.

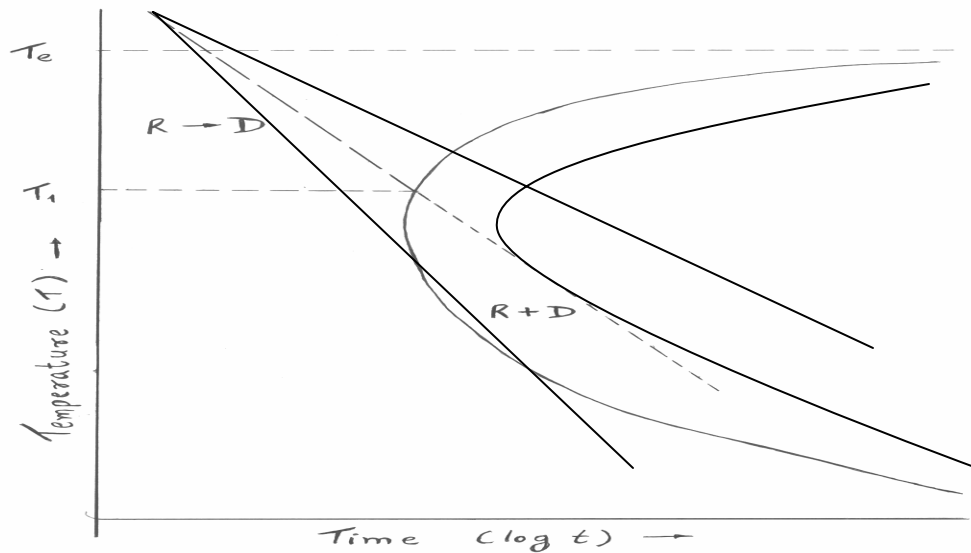


Figure-4 A TTT diagram for a process involving recrystallization and phase decomposition.

Figure- 4 indicates that the process of recrystallization has faster kinetics for isothermal treatments at temperatures between  $T_e$  and  $T_1$ . As a result it would precede the phase decomposition reaction. Thus for temperature in that range a sequential CR would produce a microstructure where phase decomposition would be observed within stress free recrystallized grains. At temperatures lower than  $T_1$  the kinetics for both reactions are comparable. This would

lead to a reaction where decomposition of the phase and recrystallization are occurring simultaneously due to a combined driving force of larger magnitude than for the individual reactions. The microstructure produced in this simultaneous mode of CR would presumably consist of phase decomposition traversing multiple grains that undergo recrystallization at the same instance. Hence, sequential and simultaneous CRs are predicted to produce morphologically significantly different microstructures.

### **2.3.3 Combined Reactions in equiatomic FePd intermetallics**

In the FePd system under consideration here, the two solid state reactions that have to be considered in terms of possible combined reactions are the ordering phase transformation and the annealing reactions, foremost recrystallization. Hence, there are two major driving forces by which a change in the microstructural state of the system can be achieved. A driving force for recrystallization is provided by the stored energy of cold work. Superimposed, is the driving force for the ordering phase transformation. Depending upon temperature of the annealing heat treatment, simultaneous or sequential CRs may be expected. Recrystallization followed by ordering (sequential) CR would be expected or at least it would be more likely at high temperatures. At small undercooling only a relatively small fraction of the large driving force for ordering would be available for the ordering transformation. For large stored strain energy this may tip the balance of the reaction kinetics in favor of recrystallization. It may be noted that at high temperatures near  $T_c$  atomic mobility should be high since volume diffusion is fairly easy. A simultaneous recrystallization and ordering CR would be expected at lower temperatures below some temperature equivalent to  $T_1$  in the example described in Fig. 4. However, a clear distinction between sequential and simultaneous reactions would be made difficult by the local

variations in driving forces. For instance, the dislocation density at some locations at the prior  $\gamma$ -phase grain boundaries and within the grains would be different in the deformed state. This could lead to different driving forces for recrystallization at different locations in the microstructure, leading to the possibility of having a sequential reaction at certain locations and a simultaneous reaction at others. Furthermore, depending on the processing parameters, annealing temperature and amount of cold work, it may be envisaged that a sequential CR begins with recrystallization and before this first reaction fully transformed the microstructure the second reaction has already begun. Thus, complexities arise in identifying the exact mode of CR, sequential and/or simultaneous. In light of these issues, a mean field approximation is assumed here for simplicity, in any attempt to develop a quantitative understanding of the evolution of microstructures in terms of the CR transformation mode.

## **2.4 COLD WORKING**

### **2.4.1 Cold Rolling**

Cold rolling is a technique used to impart controlled amount of plastic deformation. It can act as a metal forming technique and at the same time can be used to store a controlled amount of strain energy, which provides the driving force for subsequent recrystallization processes.

The true strain imparted during the cold rolling in terms of the thickness reduction can be written as [28] –

$$\varepsilon = \ln ( T_0 / T_f ) \quad \text{--} \quad (2)$$

The strain energy stored during the process of cold deformation (an approximate equation applicable for all the cold deformation techniques) is given by [8,9,13,] –

$$\Delta G^{RX} = \alpha \mu b^2 \Delta \rho / 2 \quad -- \quad (3)$$

Where  $\mu$  is the shear modulus,  $b$  is the magnitude of the Burgers vector and  $\rho$  is the dislocation density. The factor  $\alpha$  would be function of the cold working process and would account for the dislocation configuration of the cold worked state.

### 2.4.2 Equal Channel Angular Pressing

Equal channel angular pressing is a process for severe plastic deformation (SPD). It can impart a large amount of plastic deformation into the work piece without any significant change in cross section. A schematic of the ECAP process is as shown in the following fig- 5 [29]

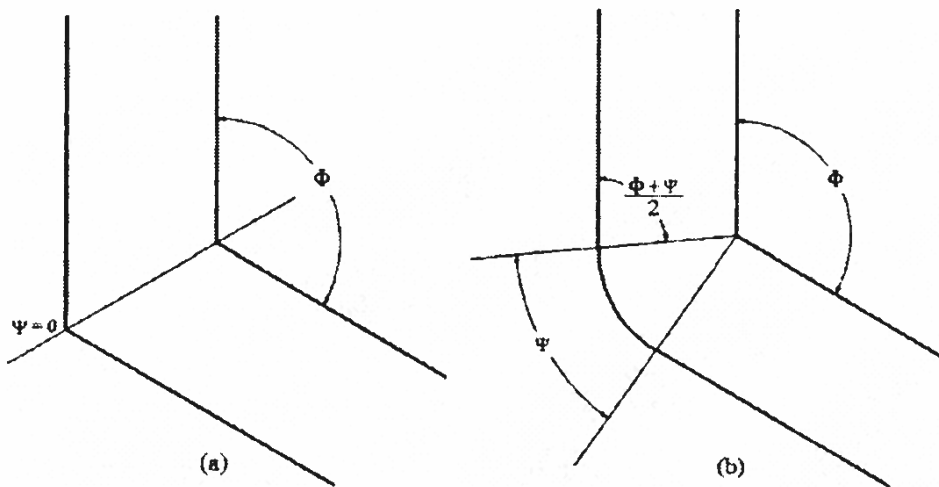


Figure – 5. Schematic for the ECAP cold deformation process a)  $\phi = 0$ , b)  $\psi > 0$

The plastic deformation is achieved by pressing a billet usually of square or circular cross-section through a die that has two channels, each with the same cross section as the billet. These two channels intersect at an angle of  $90^\circ$  or larger, which is determined by the die design. The

billet is constrained on all sides except for the opening of the second channel. While passing from one channel to the other, the material will shear along the symmetry plane lying at approximately a 45° angle of the die with an inner die angle of 90° and then flow around the corner.

The details of the processes of deformation during ECAP are controlled by the angles  $\psi$ ,  $\phi$  as defined in figure 5. The strain as a function of these angles is given by [29,30]

$$\varepsilon_{xy} = 1 / \sqrt{3} [2 \cot (\phi / 2 + \psi / 2) + \psi \operatorname{cosec} (\phi / 2 + \psi / 2)] \quad \text{--} \quad (4)$$

A highest value of strain equal to unity per pass is possible when angles  $\psi = 0^\circ$ ,  $\phi = 90^\circ$  are used. Since there is no change in the cross section of the billet during the process of ECAP, the same billet can be passed through the die again, thus increasing the amount of cumulative strain imparted to the material. Using such a multi-pass processing schedule it is possible to impart strains to the billet that have a value much larger than one. A control over the amount of cold deformation imparted to the material allows control over the driving force for the process of recrystallization available during subsequent annealing treatments. The distribution of strain, and therefore of the driving force for recrystallization, as a function of the number of passes as determined by a finite element analysis (FEA) model, using  $\psi = 0^\circ$ ,  $\phi = 120^\circ$  is shown in fig-6. The program predicts an inhomogeneous distribution of strain in the billet after one pass of ECAP with especially large strain gradients in the vicinity of the bottom surface and the front- and rear-end of the billet (figure 6). However, the central regions where strain homogeneity can be expected are also identified and increase in volume fraction with the number of ECAP passes.

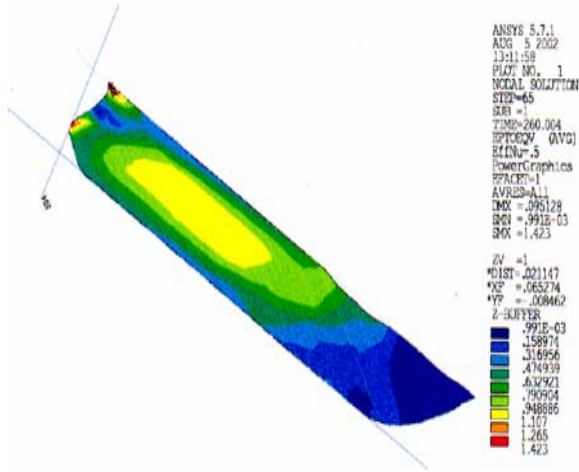


Figure – 6a

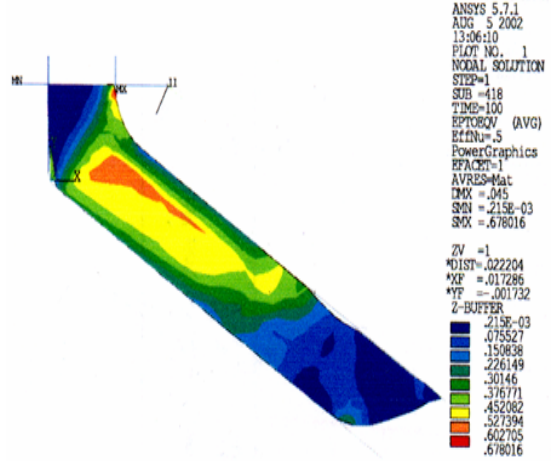


Figure – 6b

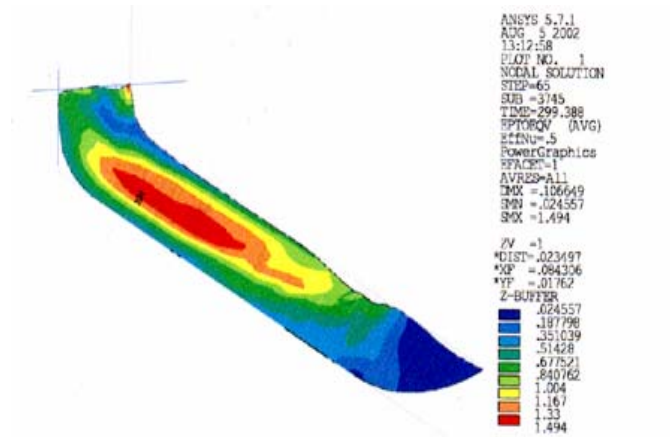


Figure – 6c

Figure-6 The distribution of strain, as determined by a FEA model , a) One pass ECAP, b) Two pass ECAP, c) Three pass ECAP.

## **3.0 EXPERIMENTAL PROCEDURE**

### **3.1 SAMPLE PREPARATION**

#### **3.1.1 Alloy preparation**

The equiatomic composition alloy was produced at Ames National Laboratory in Iowa by the Materials Preparation Center (MPC). High purity (99.99%) iron plugs were added to the required amount of high purity palladium granules (99.95%), both of which had been acquired from Alfa Aesar, to produce the equiatomic mixture. Vacuum arc melting was employed to melt the alloy followed by casting on a water-cooled copper hearth. This procedure yielded a button of approximate dimensions 45mm x 45mm x 13mm. Compositional homogeneity of the button was ensured using the EDAX compositional microanalysis in the SEM through the cross section laterally and normal to the thickness.

#### **3.1.2 Heat treatments**

To ensure controlled non-oxidizing atmosphere for heat treatments all the samples were encapsulated in quartz tubes. The same encapsulation procedure was followed for all samples. In this procedure, the samples along with a tantalum foil as an oxygen-getter were placed in the quartz tube that was sealed at one end. The tube was then thinned down with a torch, approximately 10 cm away from the closed end. The open end was then attached to a vacuum

system and pumped down to approximately 20 millitorr before back-filling with high purity argon to a pressure of approximately one-half atmosphere. The valve to the vacuum system was reopened and again pumped to 20 millitorr. This flushing procedure was repeated 4-5 times before back-filling with argon and then sealing off the tube. It was ensured that the tantalum foil and the sample are not in physical contact whilst the heat treatment was in progress.

### **3.1.3 Homogenization and Disordering Annealing Treatment**

As-cast buttons were cut perpendicular to the chill surface with a slow speed saw so that each slice had two nearly parallel surfaces. These specimens were then subjected to cold rolling to break down the cast structure. A thickness reduction to approximately 45% was achieved with the slices always going through the rollers length-wise and always in the same direction with the parallel surfaces of the samples touching the rollers. The deformed specimens were then encapsulated, and placed in a furnace at a temperature of 950°C, which is within the disordered phase field of the FePd phase diagram. After 5 hours at this temperature the quartz tubes were quenched into ice-brine solution, resulting in a relatively rapid quench to preserve the disordered phase.

## **3.2 COLD DEFORMATION**

The homogenized and disordered samples were then subjected to different mechanical processing schemes to vary the amount of stored energy of cold work.

### **3.2.1 Cold Rolling**

The disordered annealed specimens were cleaned. Billets 6mm x 6mm x 25mm in size were cut using the Struers Accutom-50 high speed cutting saw. Using multiple passes through the rolling mill, these billets were then cold rolled to a thickness of 180  $\mu\text{m}$ , approximately 97% reduction in thickness. The total effective equivalent plastic strain was calculated to be 3.0 after this cold-rolling procedure.

### **3.2.2 Equal channel angular pressing**

The disordered billets 6mm x 6mm x 25mm in dimensions were cut. These were thoroughly cleaned and lightly sanded using a 120-grit paper. An ECAP die having a 120° die angle was used for the single pass ECAP trials. The die lubricated with molybdenum disulphide was assembled and the billet was placed in the channel. Using an Instron mechanical testing machine a compressive load was applied to the billet. The test was continued until the billet passed from the entrance channel 1 through to the exit channel 2. The total effect plastic strain, using relation (2) was calculated to be 0.6

## **3.3 ISOTHERMAL ORDER-ANNEALING**

The samples for the order annealing treatment were encapsulated in quartz tubes. The single pass ECAP samples were heat treated at 400°C and 500°C. The 97% cold deformed samples were heat treated at 400°C, 500°C and 600°C. The time periods involved for these heat treatments ranged from a minimum of 1 hour at 600°C to a maximum of 10 days at 400°C.

### **3.4 CHARACTERIZATION TECHNIQUES**

#### **3.4.1 X-ray diffraction**

X-ray analysis was performed using a computer operated Phillips X'pert system operating at 40kV, 30mA and with CuK $\alpha$  radiation. Cold rolled and annealed samples with dimensions of 10mm x 10mm x 0.018mm were prepared with the rolling direction in plane. ECAP and annealed samples were prepared with a 6mm x 6mm x 1mm section of the billet perpendicular to the direction of the ECAP pass. The 'powder diffraction' technique was used for phase characterization. The powder diffraction unit consisted of a collimating slit with width equivalent to an angular width of 0.25°, a multi-purpose sample stage and a curved graphite monochromator were used to scan for the Bragg angles of the existing phases. These scans were typically run with a step size of 0.02° and the time per step of 0.8 seconds.

#### **3.4.2 Electron Microscopy**

TEM observations were carried out on samples in the deformed and the annealed state. In case of the one pass ECAP samples, the observations were made in the direction perpendicular to the direction of the pass. Whereas in case of the cold rolled and annealed condition, the TEM observations were made in the rolling plane. Discs with a diameter of 3mm were drilled out using a slurry-drill and SiC abrasive. These discs were further polished to 30  $\mu$ m in thickness and electron transparent foils were prepared using an E.A. Fishione twin-jet electropolisher in an electrolyte of acetic acid 82%, perchloric acid 9%, and ethyl alcohol 9% by volume. The electropolishing was carried out using an ice bath to cool the electrolyte to approximately 0°C. A

voltage of 30V and a jet speed of five were used. Transmission electron microscopy was conducted on the scanning TEM (STEM), JEOL 2000FX microscope operating at 200 kV and utilizing a GATAN double tilt specimen holder.

The sample preparation for scanning electron microscopy included essentially similar steps as outlined earlier. There was however no need for thickness reduction of the 3 mm diameter discs and the polishing effect of the electropolisher was sufficient to give good contrast in the backscattered electron (BSE) and the secondary electron (SE) modes. SEM investigations were conducted on a field-emission gun equipped Philips XL30 SEM, with facilities for BSE, SE contrast imaging and X-ray microanalysis using the EDAX composition analysis program.

### **3.4.3 Magnetic Measurements**

Magnetic property measurements were conducted on 3mm diameter discs with known mass. Magnetic hysteresis loops were measured using a Lakeshore model 7300 vibrating sample magnetometer. Fields approaching 15kOe were applied to the samples using a Walker laboratory electromagnet and a model 668 Lakeshore power supply. IDEAS – VSM version 2 software was used for magnetic data collation and plotting of the hysteresis loops.

### **3.4.4 Grain size analysis**

Grain size analysis was performed on SEM micrographs obtained in the BSE mode. The computer assisted image analysis procedure involved, delineating the grain boundaries, followed by a quantitative determination of the grain sizes using the NIH- image analysis software. The resolution of this grain size analysis technique was found to be in the range of 35nm and an absolute error in the estimation of grain sizes was determined to be 15nm. This error and the

resolution limits are dependent on the magnification at which the micrographs were collected and the total number of pixels of the digitally acquired images. To obtain statistical significance [31], about or more than 800 grains per treatment condition were analyzed. An example of the grain size image analysis is illustrated in figure-7.

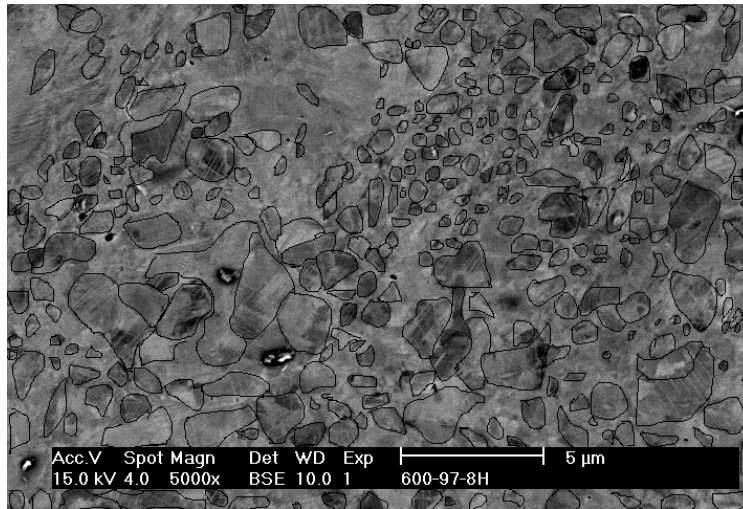


Figure-7a

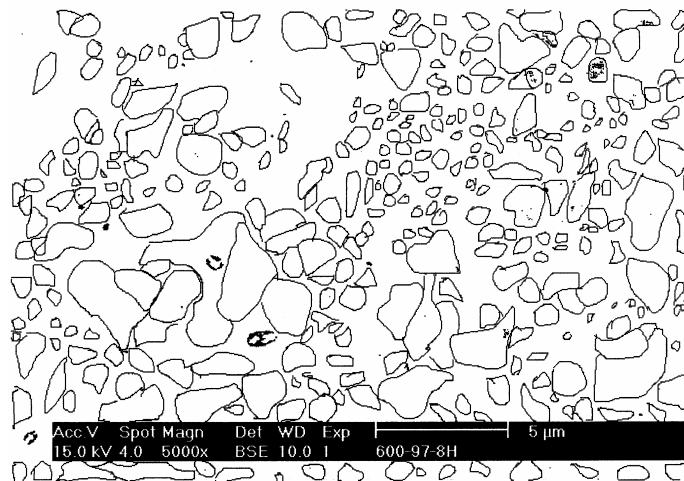


Figure-7b

Figure – 7 a) BSE, SEM micrograph with grain boundaries delineated. b) Individual grains identified by the Image analysis program and used for area determination

## 4.0 RESULTS AND DISCUSSION

### 4.1 RECRYSTALLIZED DISORDERED STATE

The microstructure of recrystallized disordered FCC FePd is as shown in fig-8. The contrast observed in this BSE - SEM image is due to differences in the crystallographic orientation. This starting microstructural state can be characterized by an equiaxed grain structure, with an approximate average grain size of  $130 \pm 5 \mu\text{m}$ . The microstructure also shows annealing twins, and well defined high angle grain boundaries. X-ray diffraction spectrum for this microstructural state shows the presence of the fundamental reflections for the disordered FCC phase. The superlattice reflections characteristic of the ordered  $L1_0$  phase were only weakly present.

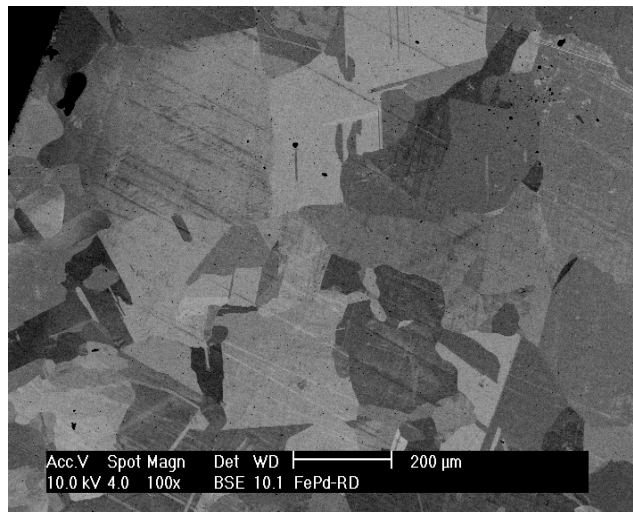


Figure – 8 BSE, SEM micrograph of disordered recrystallized Fe,Pd.

## 4.2 ONE PASS ECAP – MICROSTRUCTURE AND PROPERTY EVOLUTION

### 4.2.1 Deformed microstructure

Figures-9a and 9b show the microstructure of the alloy after one pass ECAP. After ECAP the microstructure consisted of heavily deformed grains that exhibited deformation bands at various length scales, i.e. shear, micro and transition bands. The local rotations of the crystal lattice result in fairly rapid orientation changes and a cell structure inside a given deformed grain has developed, which is reflected by the much more complex contrast in SEM BSE micrograph (figure – 9a). The TEM micrograph in figure – 9b presents a typical example of the dense defect structure developed in the deformed grains. Using diffraction contrast imaging, a dislocation density after one pass ECAP has been estimated to be  $10^{11}$ - $10^{12}$ cm<sup>-2</sup>. The accompanying SADP in figure-9b indicates the presence of a mosaic structure associated with frequent small orientation changes across the dense dislocation walls between cells of lower dislocation density. The matrix of the as deformed material has the FCC crystal structure. However, diffuse intensities for the superlattice spots in the SADP indicate the presence of L1<sub>0</sub> type either short-range order (SRO) or very small ( $\leq 2$ nm) coherent precipitates of L1<sub>0</sub> ordered orientation variants (figure-9b).

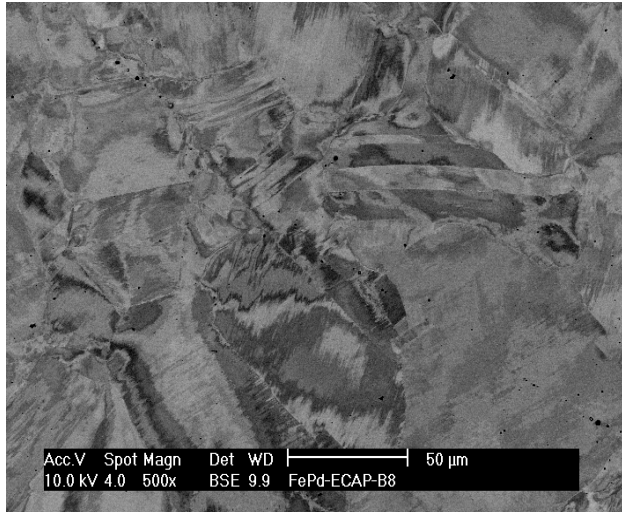


Figure-9a

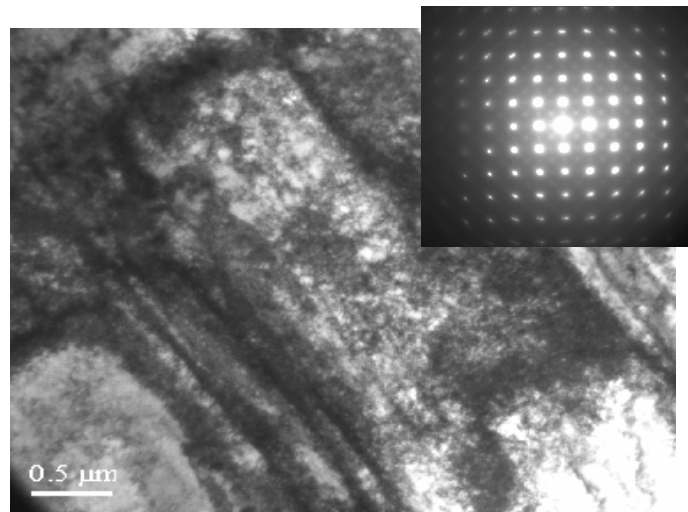


Figure-9b

Figure-9 a) BSE-SEM micrograph of disordered FePd in the deformed state after one pass ECAP. b) TEM bright field multi-beam micrograph of the dense dislocation cell structure in a grain in the FePd after ECAP, inset – SADP of the grain with a ZA of [100].

#### 4.2.2 Magnetic properties

The magnetic coercivity, a measure of the magnetic hardness, is an extremely structure sensitive property. As the processing conditions were changed the microstructure of these alloys was expected to change, which was expected to affect strongly the coercivity measured for the CR processed alloys [32].

Coercivity determination was performed using the hysteresis loops obtained with the vibrating sample magnetometer. An example of a hysteresis loop is as shown in figure-10. A demagnetizing factor of an oblate spheroid was used to correct for the demagnetizing field produced by the sample.

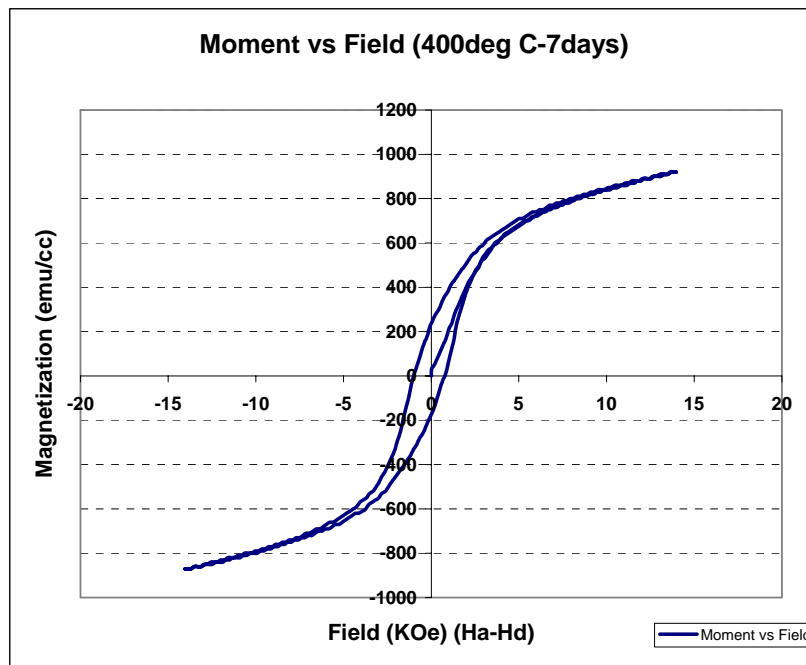


Figure -10 hysteresis loop, corrected for the shape of the sample using the demagnetizing factor for an oblate spheroid.

To monitor the development of the magnetic properties VSM experiments have been performed on the material prior to and after annealing. The evolution of magnetic hardness measured in terms of coercivity is shown in figure-11.

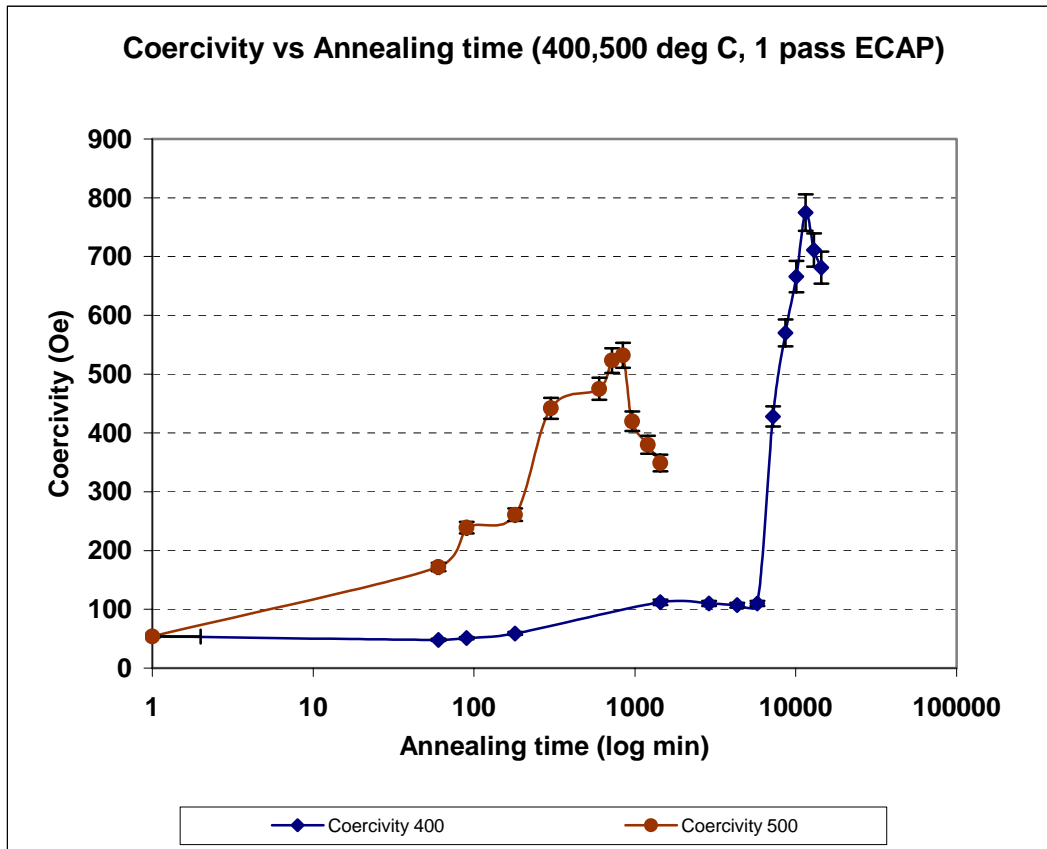


Figure-11 Coercivity evolution as a function of annealing time during order annealing after one pass ECAP

The coercivity of the as-quenched disordered FePd solid solution was 27Oe. Due to the deformation during single pass ECAP the coercivity was enhanced to 37Oe. The coercivity increased from a low value of the as-deformed state to a maximum (523Oe) after 12 hours during annealing at a temperature of 500°C. With a subsequent increase in the annealing time the coercivity was found to decrease to a low value of 349 Oe after 20 hours. A similar trend was

observed for samples annealed at 400°C with a maximum value of 775 Oe after 8 days. Previous studies have reported coercivities in the range of 180-350 for the poiytwinned microstructures that resulted during conventional transformation [8,9]. Thus, nearly a two-fold improvement in the magnetic hardness has been achieved using this thermo-mechanical processing schedule. The magnetic age hardening behavior observed in this study is consistent with previous reports, which included a different mode of cold-deformation and slightly different annealing temperatures [33]. Thus, this behavior of the coercivity with annealing time appears to be characteristic of cold-deformed FePd during annealing at  $T < T_c$ .

#### **4.2.3 X-ray diffraction – Evolution of LRO**

XRD experiments have been performed to monitor the changes of the lattice parameters during annealing. The chemical ordering sensitive  $\{113\}$  and  $\{131\}$  diffraction peaks have been used to determine changes in the (c/a) ratio or tetragonality as a function of annealing time at 500°C as summarized in figure-12. The data collated in this figure indicates that the (c/a) ratio decreases from unity prior to annealing towards the equilibrium value of 0.966 within 24 hours and remains constant thereafter. For annealing times of less than three hours the quality, peak width and signal to noise ratio, of the XRD signal was insufficient to determine with confidence apparent changes in the prominent lattice parameters. This lack of useful XRD data can be attributed to small sample size, the small fraction ordered material and the small size of the ordered domains or grains. From this data it appears reasonable to conclude that, while significant  $L1_0$  type long-range order (LRO) certainly develops within the first 5 hours of annealing at 500°C, the maximum LRO parameter is attained only after between 12 to 24 hours of isothermal annealing. The XRD analysis of samples annealed at 400°C has revealed, that the

increase in the LRO parameter is not as rapid as at 500°C. Increase to a maximum in the LRO parameter is observed after 8 days of annealing at this temperature.

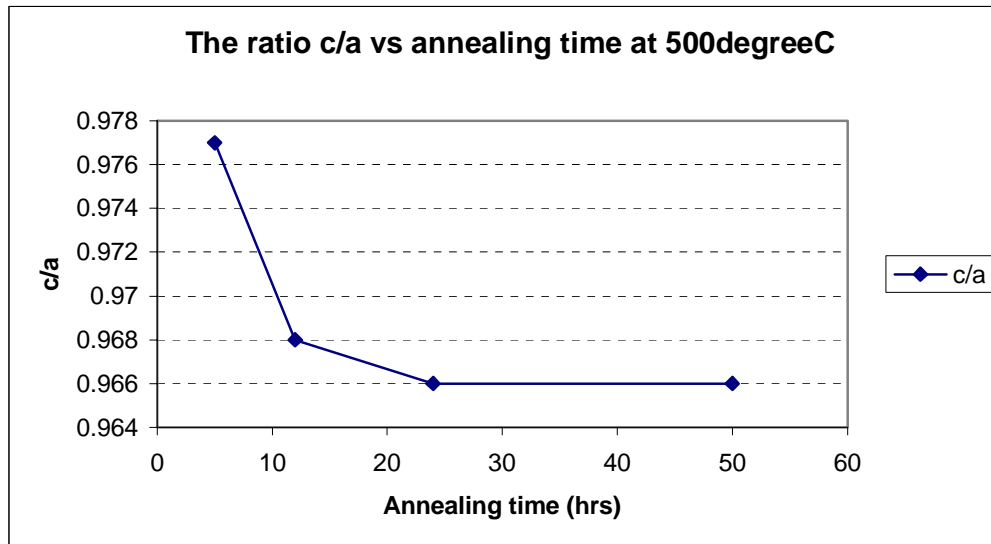


Figure -12 Evolution of the LRO parameter as a function of annealing time.

#### 4.2.4 Microstructural Observations

SEM and TEM investigations of the annealed samples have been conducted in order to document the microstructural evolution during isothermal annealing of the cold deformed FePd. TEM allows detailed local probing of structural, morphological and compositional changes on a microscopic scale. Compared to TEM, SEM studies can provide information on the microstructural evolution over much larger fields of view and also at the larger length scales. Hence by combining SEM and TEM observations, the microstructural evolution during annealing of the cold-deformed FePd could be obtained across the relevant length scales. Figure-13 and figure-14 present representative SEM,BSE micrographs that depict the pertinent microstructural features for the process of annealing at 500°C. Changes occurring in the microstructure, as a function of annealing time can be easily understood using these data sets.

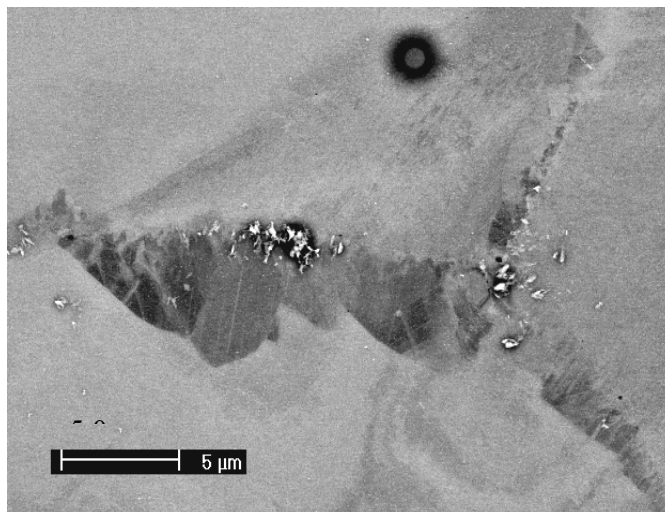


Figure -13a , 500°C-3hrs

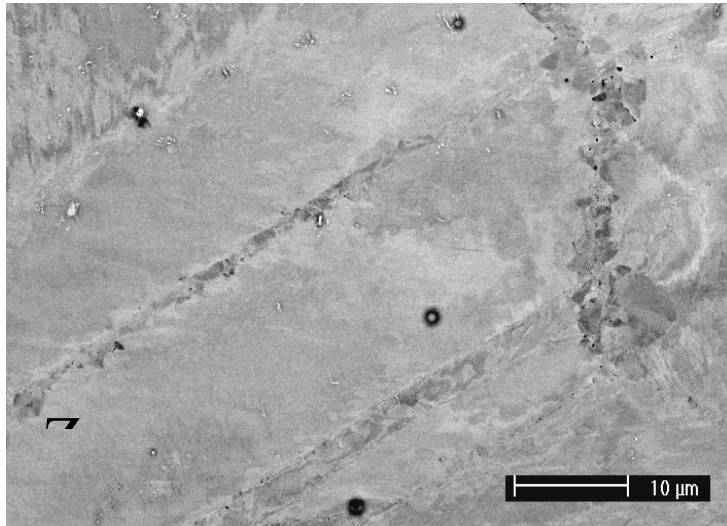


Figure -13b, 500°C-5 hrs

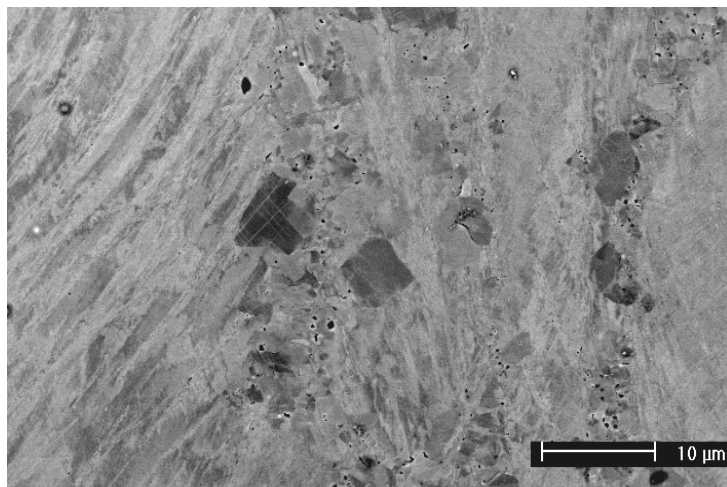


Figure -13c, 500°C-12 hrs

Figure -13 Examples of SEM BSE micrographs of the microstructural evolution in the cold-deformed Fe-Pd during annealing at 500°C a) 3 hours, b) 5 hours, c) 12 hours, c) details of CR transformed grains that nucleate at transition bands between heavily deformed regions of significantly different orientation.

As seen from the micrographs at 500°C, even at short annealing times (3hours) small, morphologically irregular shaped grains of the ordered phase emerge initially at grain boundaries (GBs) of the disordered, deformed FCC phase. These new grains appear to be the product of a concomitant recrystallization and ordering process, a combined reaction process (CRP) that has characteristics of being a nucleation and growth type process. It can be seen from the microstructure in figures-13 that the grains of the deformed matrix do not undergo any morphological changes that can be classified as an annealing phenomenon. Figure – 13b depicts an example of the microstructure after 5 hours of annealing. A significant fraction of CR transformed grains has nucleated at micro-bands within a non-CR transformed grain in addition to CRP grains at grain boundaries. With increasing annealing time, this process of heterogeneous nucleation of CRP grains at GBs and deformation bands and their growth into the surrounding non-transformed volume continues. Figure-13c depicts an example of CRP grains at transition bands, which separate regions of differently oriented deformed crystal with shear bands. Planar faults such as twins can be seen in the larger grains in the CR transformed fraction. Furthermore the CR fraction consists of a large number of grains having an average diameter in the sub-micron scale. Comparison of figures from 13a-13c reveals that the CR transformed fraction in these alloys increases with increasing annealing time.

Quantitative studies on these micrographs using computer assisted image analysis has shown that the CR transformed fraction increases from about 2% after 3 hours to 36% after 12 hours of annealing at 500°C and reaches a maximum of 45% after 24 hours of annealing. A completely CR transformed state was not observed even after 24 hours of annealing at this temperature. This observation has implications in defining an adequate driving force for the process of

recrystallization during CR transformation. Apparently the driving force imparted by one pass ECAP was not sufficient to effect a combined reaction process throughout the matrix.

Figure –14 presents SEM micrographs of the microstructures typical of annealing at 500°C for

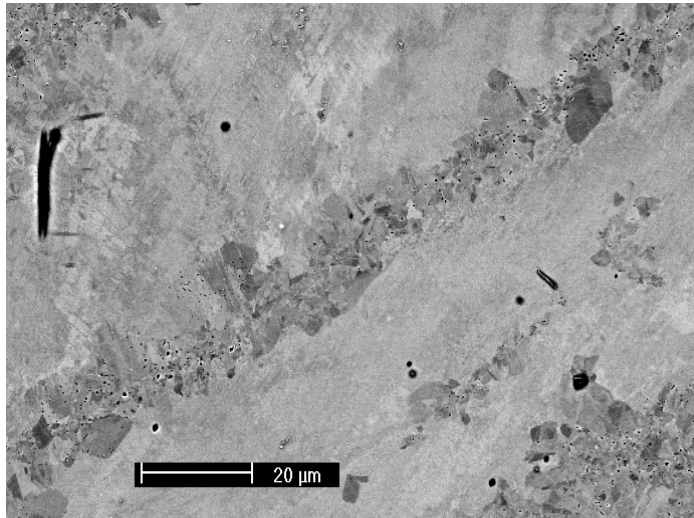


Figure-14a, 500°C-12 hrs

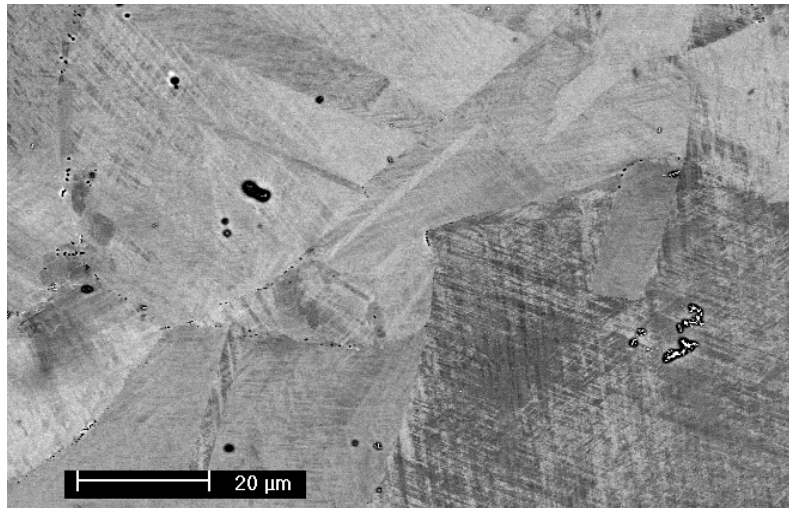


Figure-14b, 500°C-24 hrs

Figure-14 SEM, BSE micrographs of the microstructures after a) 12 hours and b) 24 hours of annealing at 500°C.

12 hours and 24 hours. While microstructural morphology, namely heterogeneously distributed, irregularly shaped CRP grains and a majority volume fraction of non-CR transformed grains remained essentially the same up to 12 hours of annealing, a significantly different microstructure appeared after 24 hours of annealing. The microstructure in this state appears to be more homogeneous, since the heterogeneously distributed small CRP transformed grains that decorated the GBs and the deformation bands within the non-CR transformed grains are no longer observed (figure-14b). Instead, many larger CR transformed grains that contain annealing twins along with non-CR transformed regions that appear to contain polytwins are seen in the microstructure. A significant size difference in the largest grains observed in the CR transformed regions is also seen. While the largest grain size after 12 hours of annealing was in the range of 10  $\mu\text{m}$ , after 24 hours most CR transformed regions had grown to a size range of about 80  $\mu\text{m}$  on average. It appears likely that this change in CRP grain size and in microstructural morphology is associated with the suppression of further transformation of deformed regions by the CR and the rapid growth of select grains in the population of CRP transformed grains between 12 and 24 hours of annealing. A semi-quantitative (insufficient statistics) grain size distribution analysis in the CR transformed fraction has revealed a quite heterogeneous distribution. It therefore appears reasonable to envisage that the larger grains in the CR transformed regions, under the driving force of reduction in excess surface energy, would grow at the expense of smaller ones.

The microstructural data imply that the fraction CR transformed increases monotonically with annealing time until completion of the ordering transformation. However, even after 24 hours the fraction transformed does not increase beyond 45%. Thus, it would be rational to expect that the magnetic age hardening behavior does not depend solely on the increment of fraction CR transformed. Interestingly the maximum in coercivity observed after 12 hours at 500°C correlates

well with the time required to achieve a LRO parameter close to unity. This observation implies that the increase in coercivity can be attributed to an increase in the LRO parameter in the overall microstructure. The decreased coercivity for annealing times longer than 12 hours appears to correlate with the significant grain growth in the CR transformed fraction of grains and the accompanying change in microstructural morphology.

TEM studies have been conducted on the partially ordered and completely ordered states. The TEM micrographs in figure-15 have been obtained from non-CR transformed regions after annealing for 5 hours and 24 hours at 500°C.

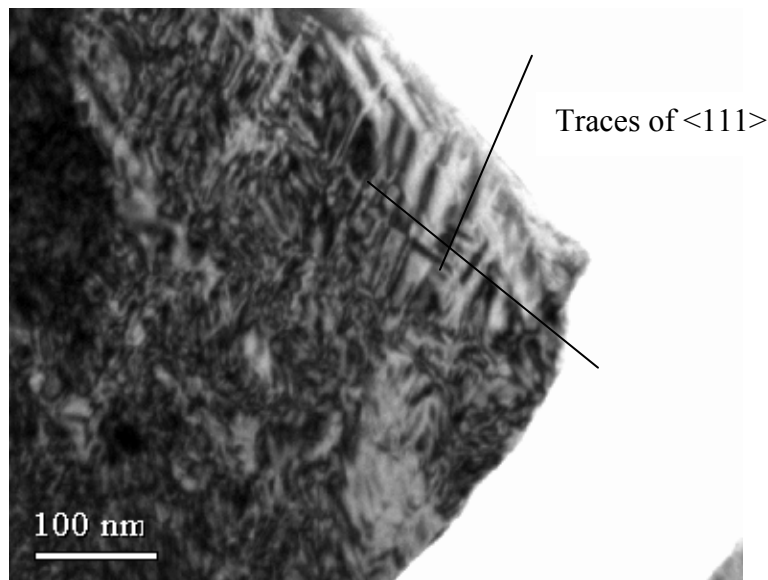


Figure -15a

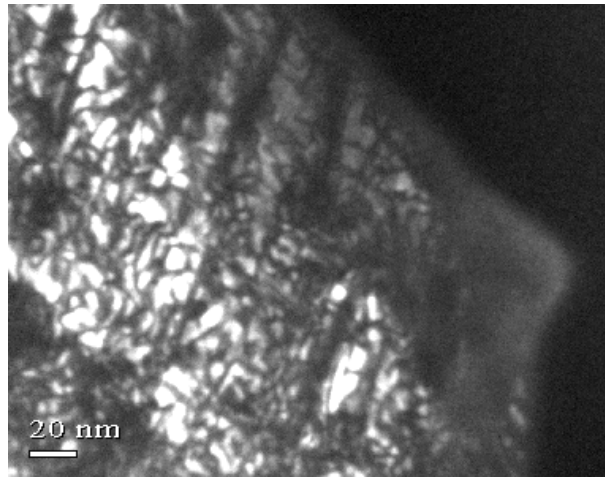


Figure – 15b

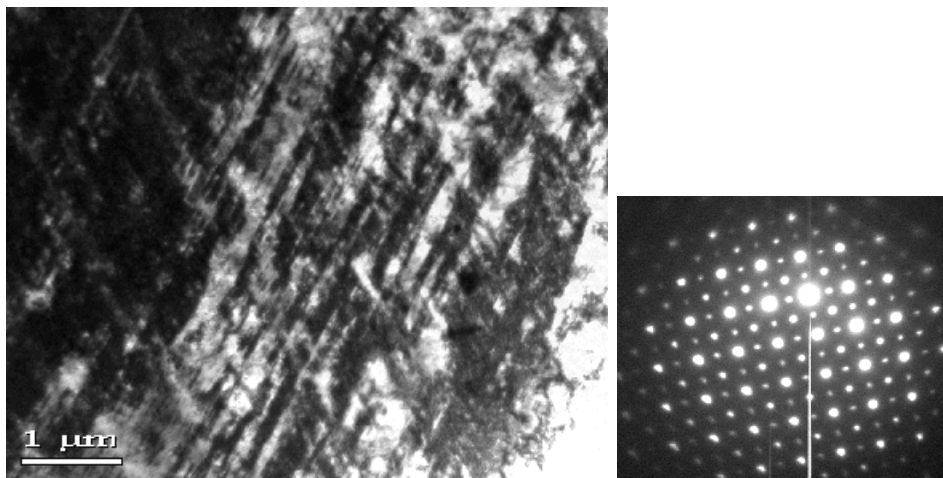


Figure -15c

Figure – 15 Example TEM micrographs depicting the evolution of L10 – type LRO in the non-CR transformed region. a) Bright field,  $g = 002$ , off  $[110]$ , b) corresponding dark field with  $g=001$ , both for 5 hours annealing at  $500^{\circ}\text{C}$ . Traces of dodecahedral planes parallel to  $[1-11]$  and  $[1-1-1]$  are marked in a). c) multibeam bright field, beam direction  $[001]$ , inset SADP, for 24 hours of annealing at  $500^{\circ}\text{C}$

The complex contrast observed in these micrographs is due to the nucleation and growth type conventional ordering reaction occurring within these regions [3]. The FCC  $\rightarrow$  L1<sub>0</sub> phase transformation is associated with a characteristic transformation strain. Under the influence of this strain the product of this reaction assumes a lamellar morphology and aligns itself approximately parallel to the traces of dodecahedral planes, namely the directions [1-11] and [1-1-1] as depicted in the micrograph of figure 15a. The superlattice dark field TEM micrograph of figure-15b shows the same region as 15a, but at a higher magnification, revealing the nanoscale coherent precipitates of one of the three orientation variants of the L1<sub>0</sub> ordered phase emerging within the FCC matrix. Under the influence of the transformation strain, variant selection occurs locally during growth and small coherent L1<sub>0</sub> precipitates coalesce to form larger ordered domains aligned parallel to the traces of dodecahedral planes. These observations are consistent with the emergence of an incipient polytwin structure in the non-CR transformed grains during annealing of the cold-deformed FePd. The continued ordering and coarsening of these aligned ordered domains during isothermal annealing at this temperature produces a fairly well developed polytwin structure in the non-CR transformed grains after 24 hours. The accompanying [001] ZA SADP inset in figure-15c exhibits eight superlattice spots surrounding the central spot, which indicates the presence of all three possible orientation variants of the tetragonal ordered phase in the non-CR transformed grain.

An example of heterogeneous nucleation and growth of CR transformed grains at the GB between two formerly disordered, deformed grains is given in the TEM micrograph, figure – 16. Diffraction studies of these heterogeneously nucleated CR transformed grains indicate that these grains are essentially defect free and have an ordered  $L1_0$  structure. Microstructural observations similar to the 500°C isothermal annealing treatment have been made at a lower annealing temperature of 400°C. The main difference in the evolution of the microstructure is the considerably slower reaction rate at this lower processing temperature. This has resulted in a peak in coercivity and a corresponding increase in the order parameter to a value of unity after a time period of 8 days at 400°C.

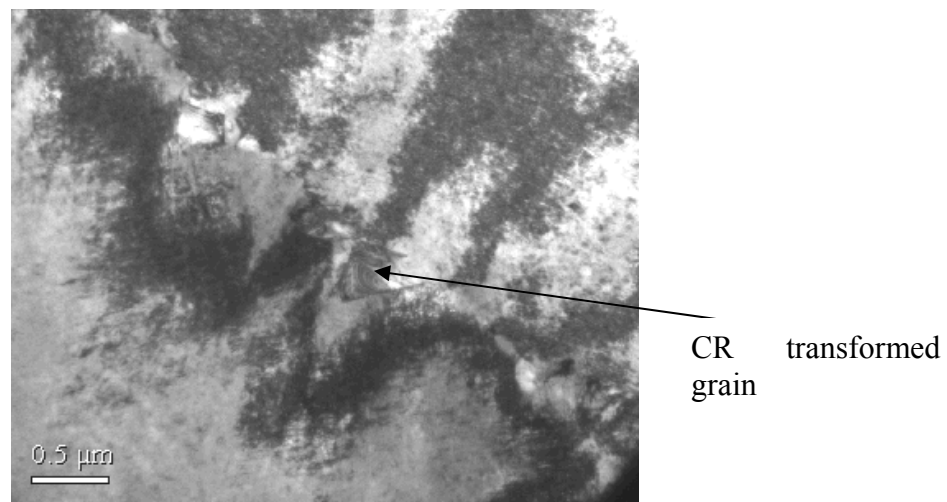


Figure -16 Multi-beam bright field TEM micrograph depicting an example of new  $L1_0$  – ordered CRP grains, in the cold-deformed Fe-Pd after 10 hours of annealing at 500°C

#### 4.2.5 Discussion

Microstructural evolution –

The observations of the microstructural evolution are in accordance with expectation for a low stacking fault energy material [34,35,36]. For instance the large strain energy gradient present at the deformation bands and at high angle grain boundaries in the deformed microstructure provides sufficient driving force for preferential nucleation of defect free, recrystallized grains. Of the various recrystallization mechanisms previously enumerated, based on microstructural observations (e.g. figure-13), it would be tempting to consider a pure recrystallization mechanism where the nucleation of a stress free grain would occur by a bulge mechanism [13,35] (essentially similar to the stress-induced boundary migration (SIBM) mechanism).

However, the system under consideration undergoes a recrystallization and a concomitant phase transformation. Thus, the local variations in the defect content would have to be considered, while trying to understand the microstructural evolution from a disordered, deformed FCC to an ordered L1<sub>0</sub> state.

The energy barrier for nucleation of the ordered L1<sub>0</sub> phase can be given by [37]

$$\Delta G^* = (16 * \pi * \gamma^3) / (3 * (\Delta G + \Delta G_d)^2). \quad -- \quad (5)$$

The reduction in free energy due to the FCC → L1<sub>0</sub> phase transformation ( $\Delta G$ ) is aided by a reduction in free energy due to elimination of defect content ( $\Delta G_d$ ). Consequently a smaller energy barrier to phase transformation would be present in regions of high defect content (due to a larger  $\Delta G_d$ ). This would in turn lead to preferential nucleation of the L1<sub>0</sub> phase at locations with high defect content, such as deformation bands and prior high angle grain boundaries. The experimentally observed microstructures do depict these kind of discontinuous, nucleation and

growth events (figure-10, 11), which lead to monolithic, single variant, defect free grains. As previously stated the ordering phase transformation is associated with a transformation strain and a strain accommodation among all three possible  $L1_0$ -variants nucleated produces the polytwinned structure. However, in case of the CR transformed grains, only a single variant is observed. This observation can be rationalized based on the fact that the transformation strain can in itself be accommodated by the interaction of the moving high angle grain boundary with the surrounding non-CR transformed, heavily defected region.

The defect content within the grains of the deformed FCC phase is considerably lower than at the high-strain energy concentration locations, such as at prior GBs and micro and transition bands. Thus, in the absence of or for a significantly reduced magnitude of the additional driving force  $\Delta G_d$ , the probability of nucleation of  $L1_0$  phase is reduced. Furthermore, inside the deformed FCC grains the probability for nucleation of any of the three possible  $L1_0$ -variants appears to be about equal. Thus, an ordering process similar to the conventional mode typical of the undeformed material, which favors the nucleation of all three variants is expected within the matrix. While somewhat speculative, the observations are consistent with this scenario (figure-12, 13). The regions referred to as a non-CR transformed region, indeed show the presence of polytwinned structure consisting of all three variants.

During early stages of the annealing process there is a competition between the conventional and the heterogeneous or CR ordering modes. The resulting microstructure is therefore a composite, comprised of regions that have CR transformed and regions that have transformed by the conventional mode. The driving force for phase transformation vanishes once the LRO achieves the equilibrium value. Coincidentally, this occurs apparently when the maximum in coercivity is attained. During subsequent annealing only the driving force for grain growth is present. Under

these circumstances reduction in excess surface energy leads to grain coarsening in the fully ordered material.

Magnetic property evolution -

Based on the magnetic property measurement, a magnetic age hardening behavior has been reported for these thermo-mechanically processed intermetallics. In the initial stages of annealing the coercivity increases monotonically to a maximum (523 Oe) followed by a decrease to values typically in the range of those obtained for conventionally processed FePd. This behavior has been observed to be consistent with previous work [5,33]. XRD data has confirmed the correlation between the increasing coercivity and the increasing order parameter (LRO). However subsequent magnetic ‘overaging’ cannot be attributed to the LRO parameter, as with increasing annealing time, this parameter monotonically increases towards unity and remains constant upon completion of the ordering transformation. Similarly, the fraction CR transformed was found to increase monotonically even at the onset of overaging. Thus, the characteristic magnetic age hardening behavior of cold-deformed FePd cannot be attributed solely to the evolution of LRO and / or the evolution of the fraction CR transformed.

The microstructure associated with the maximum in coercivity has CR and non-CR transformed regions in it. The CR transformed regions are essentially defect free and consist of monolithic  $L1_0$  ordered, equiatomic FePd grains, which are considerably smaller in size (submicron range average grain size). These grains are surrounded by non-CR transformed fraction that exhibits polytwinned morphology.

It has been proposed [8] that the increased coercivities of CR processed FePd originates from a superposition of magnetic hardening mechanisms that take into account the contribution to coercivity from greatly reduced grain size (grain size hardening) and by pinning of magnetic

domain walls by planar defects. According to previous reports [8] the grain size hardening contribution to the coercivity enhancement,  $\Delta H_D$ , in combined reaction transformed FePd can be given by approximately

$$\Delta H_D = (\beta \gamma / D M_s) \text{ --} \quad (6)$$

Where  $\beta$  is a geometrical factor with a value between 1 to 5,  $\gamma$  is the domain wall energy (17erg/cm<sup>2</sup>),  $M_s$  is the saturation magnetization (1100emu/cm<sup>3</sup>) and  $D$  is the average grain size.

Considering the range for  $\beta$  and a grain size of 1 $\mu$ m, the approximate upper and lower bounds of  $\Delta H_D$  are estimated to be about 155 Oe to 775 Oe. For grain sizes 30  $\mu$ m or larger the grain size hardening effect becomes negligible. After 24 hours at 500°C (that is in the significantly overaged condition), the CR transformed fraction was seen to be about 45% and an average CR transformed grain size was measured to be 80  $\mu$ m. Using above model, the contribution to coercivity from these CR transformed grains that have undergone considerable grain growth, would be very small (on the order of 10-25Oe).

Microstructural observations have also indicated that the defect density in the non-CR transformed matrix is considerably reduced during the process of annealing. Potent line defects such as dislocation tangles can act as pinning sources to moving 180° domain walls. Due to a reduction in the density of these defects with increasing annealing time, a reduction in the pinning contribution to coercivity would be expected, thus decreasing the overall magnetic hardness. While quantitative description of the reduction in pinning strength is not possible due to the local variations in the defect density in the microstructure, however it can aid in qualitative understanding of the reduction in magnetic hardness.

Hence it appears reasonable to conclude that the significant grain growth in the CR transformed fraction is responsible for the observed drop in coercivity in the overaged condition.

### **4.3 COLD ROLLED TO 97% REDUCTION IN THICKNESS – MICROSTRUCTURE AND PROPERTY EVOLUTION.**

In an effort to further optimize the magnetic properties, while exploring the matrix of processing parameters of annealing temperature, annealing time and stored strain energy of cold work, cold rolling to 97% reduction in thickness was employed. The process of cold rolling is capable of imparting a large amount of strain energy to this relatively ductile material. The calculations in section 3.2.1 show that under these conditions the total equivalent effective strain imparted to the material is larger than that calculated for a single pass ECAP, namely 3.0 versus 0.6 for deformation by cold rolling and ECAP, respectively. The increased amount of stored strain energy of cold work after cold rolling compared to the single ECAP pass would provide a larger driving force for recovery and recrystallization [13]. The thermo-mechanical processing by cold rolling would be expected to alter the kinetics of the CR transformation. Thus, the microstructural state after CR transformation in the cold rolled intermetallics would be predicted to differ from that in the material processed by a single pass ECAP. These changes in microstructure are also expected to alter the evolution of the coercivity or magnetic age hardening behavior, in terms of the rate of approach to the maximum, the maximum value, and the rate of overaging.

### 4.3.1 Deformed microstructure

Figure – 17 shows an example of the deformed microstructure after cold rolling to 97% reduction in thickness.

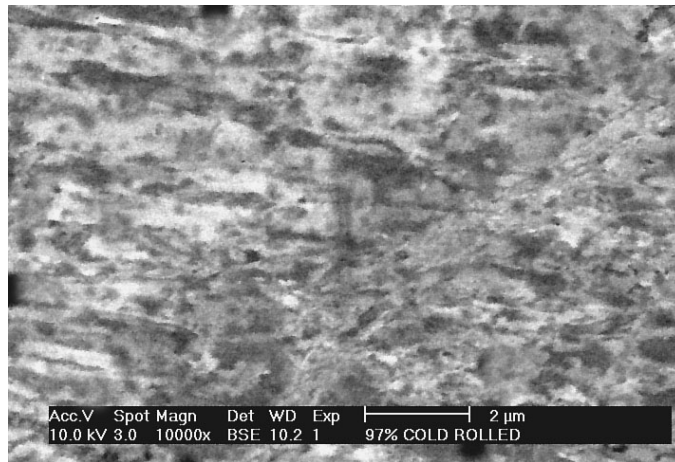


Figure -17 BSE, SEM image of the microstructure in the cold rolled to 97% reduction in thickness sample.

The contrast in this BSE image is based only on variations in local crystallographic orientations since there are no significant compositional changes associated with the transformation of the equiatomic Fe-Pd during annealing. Due to the large amount of deformation a very high density of dislocations is expected to be present in the microstructure and the crystal lattice orientations change over a rather small length scale comparable to the resolution of the SEM micrograph of figure-17. The internal stress fields associated with the high dislocation density of the as-deformed microstructure results in rather diffuse contrast in the backscatter electron (BSE) mode. As described previously the microstructure in the deformed condition includes deformation, shear-, micro- and transition bands (see section 4.2.1). The development of a

dislocation cell structure in the alloy after cold rolling can also be inferred from the micrograph of figure-17. A much larger dislocation density is expected within the cell walls and at intersections of cell walls than in the cell interiors. Usually the dislocation cell-structure consists of cell interiors that are relatively dislocation-free and the cell-delineating cell walls that contain very high densities of dislocations. Hence, while the overall average dislocation density is of course increased by the increase in strain of cold-work, the dislocation density,  $\rho(r)$ , is not homogeneous at the scale of the cell-structure. Regions of elevated local dislocation density within the well-developed cell-structure might be expected to act as preferential sites for nucleation of CR transformed grains.

#### **4.3.2 Magnetic properties**

Figure-18 summarizes coercivity measurements extracted from magnetization versus external applied field or M-H loop type magnetic hysteresis magnetization-demagnetization experiments performed on isothermally annealed samples.

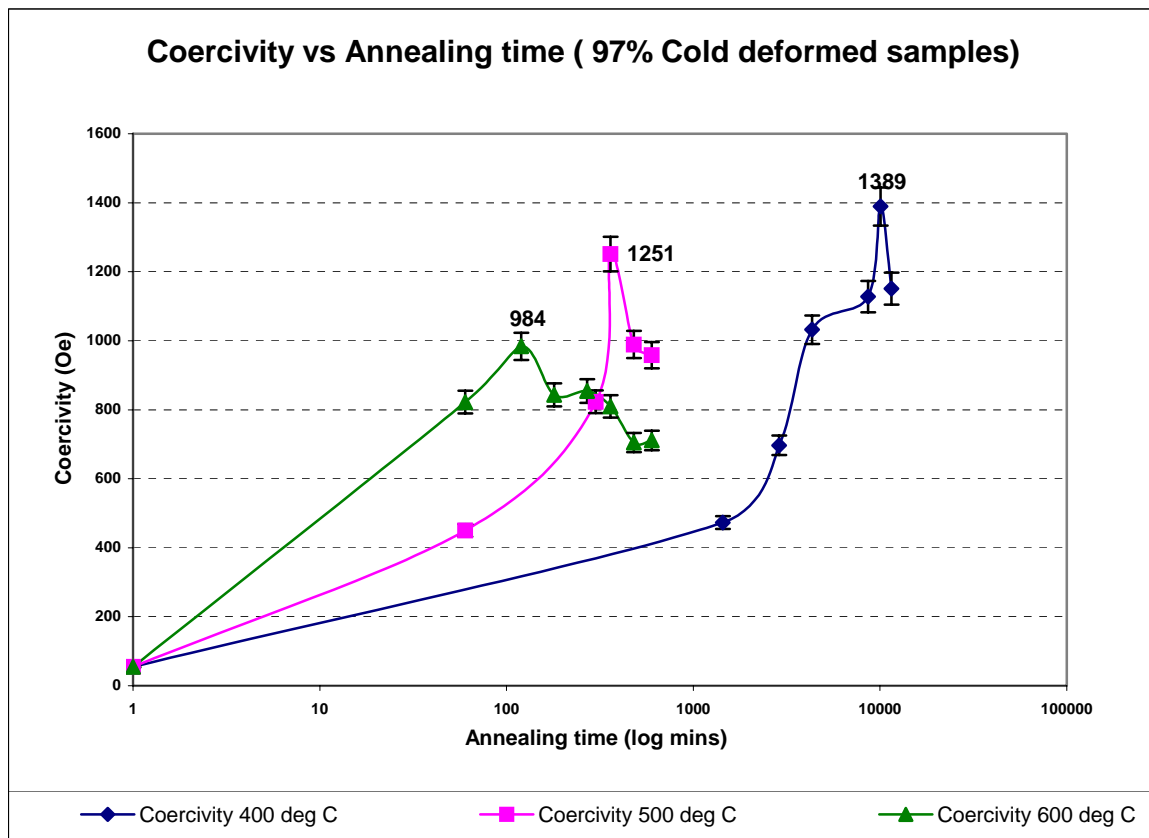


Figure -18 Coercivity evolution as a function of annealing time during order annealing after 97% reduction in thickness by cold rolling.

These experiments have been performed in a vibrating sample magnetometer (VSM), with the rolling direction aligned parallel to the externally applied field. In order to assess the potential effect of crystallographic textures, VSM measurements have been performed for systematically varied orientations of the applied field relative to the RD of the samples. The coercivity values obtained in these experiments have been found to be essentially the same (e.g a range of  $H_c$  between 1251 Oe and 1237 Oe obtained for the maximum coercivity condition after 6 hours at 500°C). This implies that the effect of microstructural textures, which may have developed

during CR transformation, do not have a significant effect on the magnetization behavior measured by VSM.

Figure-18 depicts the characteristic magnetic age-hardening behavior observed for all the isothermally annealed samples. These observations are similar to the coercivity behavior after one pass ECAP. However, relative to the polytwinned microstructure a five-fold increase in the maximum coercivity is observed, while for the single pass ECAP only a two-fold increase was obtained. Furthermore, the time required to reach the maximum in coercivity is also reduced by the larger cold-deformation strain. For instance, during the 500°C isothermal treatments the maximum is reached after 6 hours for the larger strain imparted by cold rolling, while it took 12 hours to reach maximum coercivity for the lower strain deformation by one-pass ECAP. However, comparable annealing time is required for the attainment of a maximum coercivity at 400°C for the two different levels of strain of cold-work. These observations have their origin in the kinetics of the processes facilitating the microstructural transformation and are discussed in more detail in the following sections.

#### **4.3.3 X-ray diffraction – Evolution of LRO**

From studies of the evolution of the long-range order parameter for the single pass ECAP samples, during the isothermal treatment at 500°C, it was concluded that the ordering process is essentially complete when the maximum in coercivity is obtained. XRD experiments have also been conducted to study the LRO evolution in cold rolled and annealed samples. Figure-19 depicts a representative set of a symmetric ( $\theta$ -2 $\theta$ ) XRD scan obtained for cold rolled samples annealed at 600°C for a time period at which a maximum in coercivity is observed (3 hours).

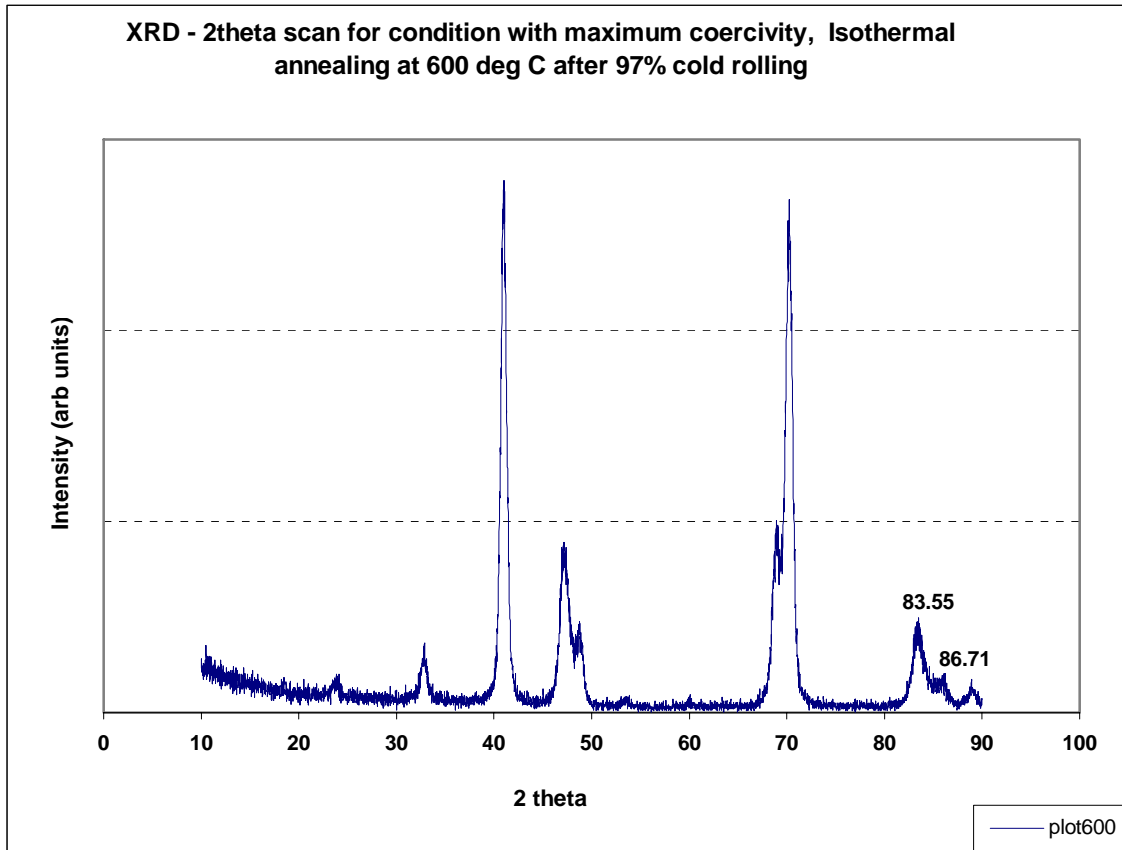


Figure-19 Representative set of a symmetric ( $\theta$ - $2\theta$ ) XRD scan obtained for cold rolled samples annealed at 600°C for a time period at which a maximum in coercivity is observed (3 hours)

Peak splitting can be observed in this XRD scan. Diffraction peaks (001) at  $2\theta \sim 24.5^\circ$  and  $\{110\}$  at  $2\theta \sim 34^\circ$ , as well as the splitting of the  $\{200\}/\{002\}$  pair of peaks around  $2\theta \sim 48^\circ$  and the pair of peaks  $\{220\}/\{022\}$   $2\theta \sim 70^\circ$ , all bear evidence of the transformation to the tetragonal  $L1_0$  – ordered phase.

Due to the typical effects of the geometry using a diffractometer set-up for the XRD experiments better accuracy in d-spacings is obtained at higher scattering angles. Hence, here the intensity distributions corrected for the multiplicity factor, which accounts for the effects of tetragonal

symmetry of the ordered structure, have been analyzed for split peaks at larger values of  $2\theta$  close to  $90^\circ$ . The family of  $\{113\}$  and  $\{311\}$  peaks shows splitting at the largest values of  $2\theta$  ( $\sim 85^\circ$ ) in the XRD scan, and thus these peaks have been employed to determine the  $c/a$  ratios as a function of annealing time for a given isotherm.

To summarize briefly these XRD data analyses, here the computed  $c/a$  ratios from data collected for the various annealing temperatures for the condition of maximum coercivity are collated in table –2.

Table – 2  $c/a$  ratios obtained for the condition of maximum coercivity at various annealing temperatures.

Temp.	2theta	peak	c/a
400 deg C	83.01	{311}, {131}	0.9660 +/- 0.0005
	86.51	{113}	
500 deg C	83.21	{311},{131}	0.9660 +/- 0.0005
	86.57	{113}	
600 deg C	83.55	{311}, {131}	0.9660 +/- 0.0005
	86.71	{113}	

Clearly, within the conservatively estimated experimental error of these measurements the LRO parameter, as represented by the  $c/a$  ratio, has reached the equilibrium value for the microstructural conditions associated with maximum magnetic coercivity. At shorter times of annealing values of  $c/a$  closer to unity have been observed for all annealing temperatures. Thus, it appears reasonable to conclude that the ordering process is essentially complete when a maximum in coercivity is attained during annealing of the cold rolled FePd. The achievement of

the long-range order is intimately linked with the microstructural evolution, and will be discussed in greater details in the following sections.

#### **4.3.4 Microstructural Observations**

Apart from using XRD to monitor the evolution of LRO, the evolution of the microstructural state has also been documented using SEM and TEM. SEM provides a larger area overview of the microstructure and therefore aids in understanding the evolution of microstructure over a larger and perhaps more representative length scale than TEM. Information about important microstructural metrics, such as average grain size, the density of planar defects, such as annealing twins etc., can be obtained from these micrographs. TEM on the other hand provides a much better tool to probe the local morphology and crystallography of the microstructure. Using both these tools in conjunction, it is possible to obtain insight on the microstructural evolution spanning a rather wide length scale range of  $\sim 10^{-3}$  m to  $10^{-9}$  m.

An example of an SEM BSE micrograph for a condition of partial CR transformation of the cold rolled FePd is shown in figure – 20

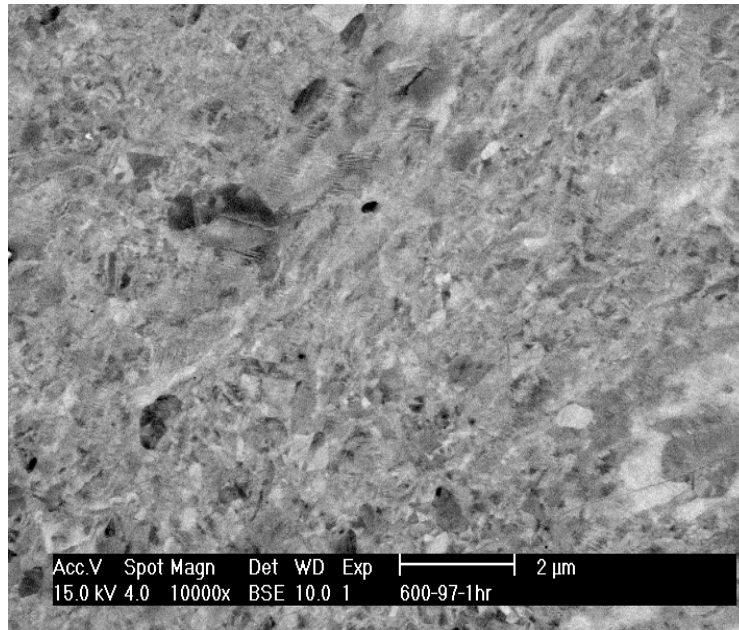


Figure -20 BSE, SEM micrograph showing a microstructural state that has been partially transformed by CR process.

Clearly, the microstructural state is complex in the partially transformed state. There are regions in the microstructure, which appear to have transformed by the heterogeneous nucleation and growth of CR grains. These nucleation and growth events seem to be aided by the prior deformation induced defect content. These observations of the microstructure in the early stages of the magnetic age hardening curve after cold rolling are in qualitative agreement with observations made for the partially transformed samples deformed by a single pass of ECAP.

Examples of SEM BSE micrographs for annealing conditions associated with the maximum in coercivity and in the magnetically overaged condition for the three isothermal annealing temperatures explored are shown in figures – 21, 22 and 23. These micrographs are representative of a much larger group of observations made on much larger fields of view for each of the different annealing conditions.

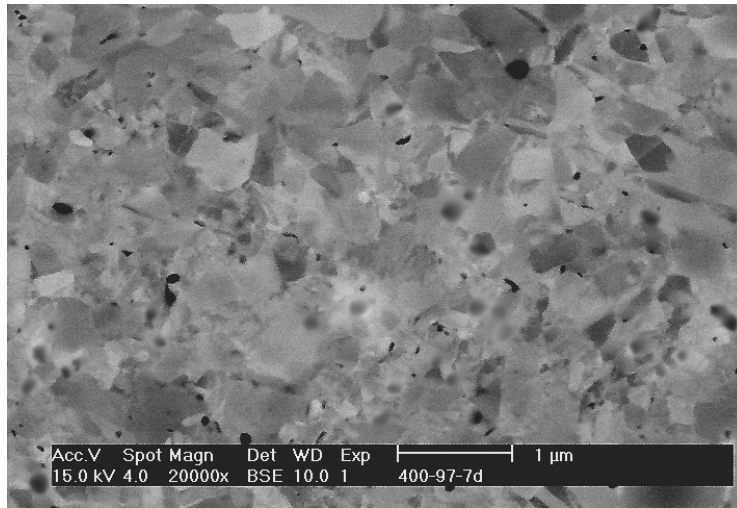


Figure-21a

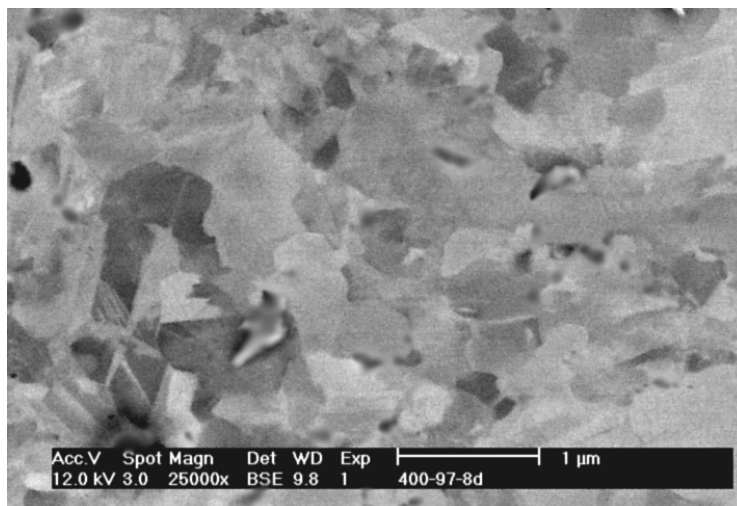


Figure-21b

Figure-21 BSE, SEM images of the microstructure after annealing at 400°C a) at the peak in the magnetic age hardening curve – annealed for 7 days; b) in the overaged condition – annealed for 8 days.

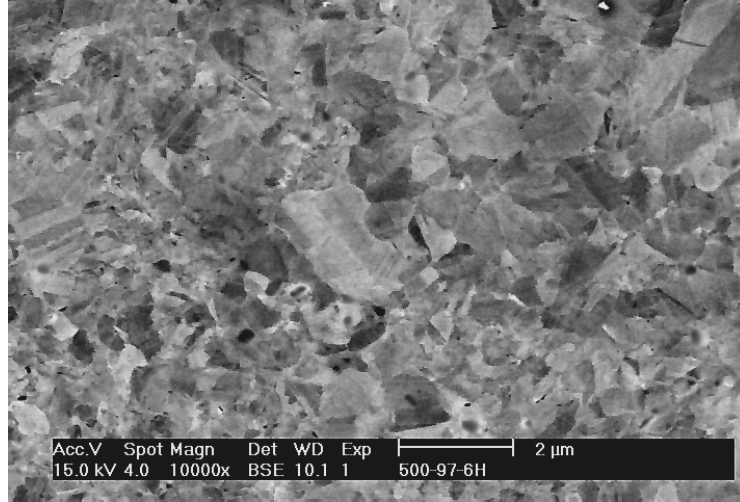


Figure -22a

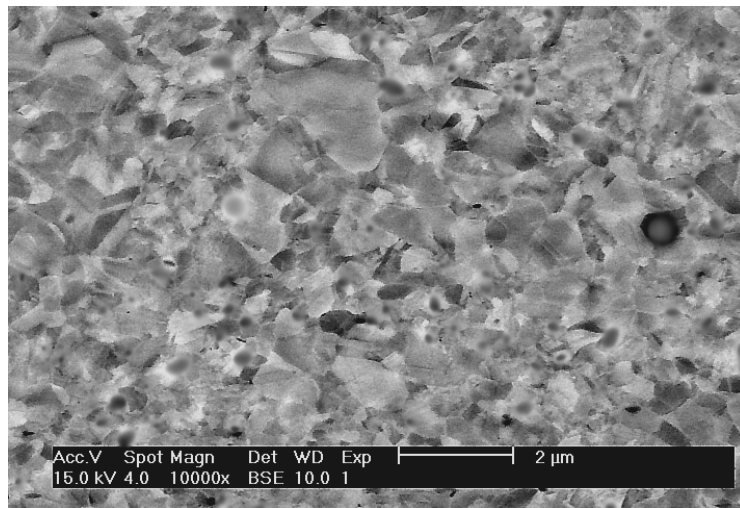


Figure -22b

Figure-22 BSE, SEM images of the microstructure after annealing at 500°C a) at the peak in the magnetic age hardening curve – annealed for 6 hours, b) in the overaged condition – annealed for 10 hours.

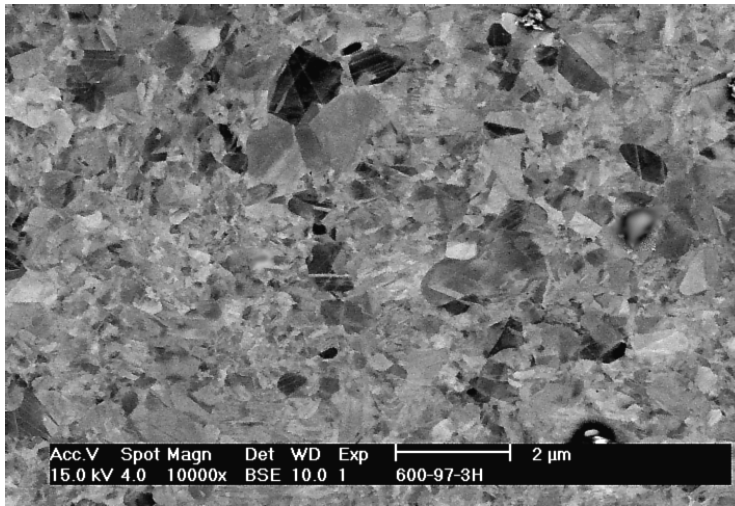


Figure-23a

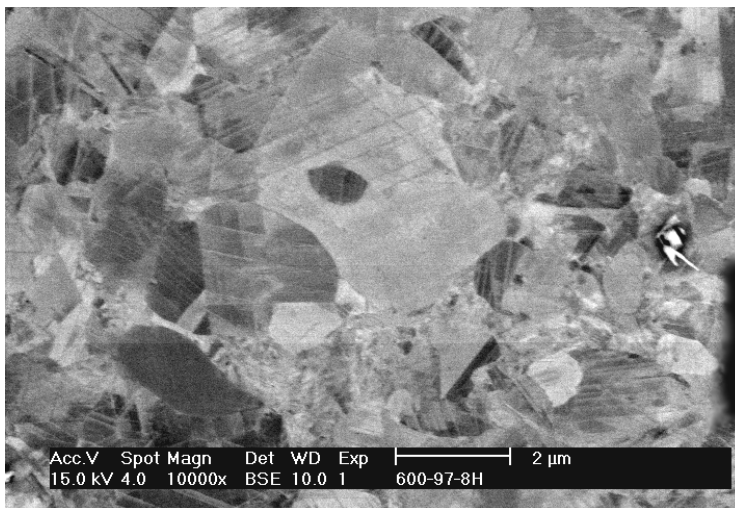


Figure-23b

Figure-23 BSE, SEM images of the microstructure after annealing at 600°C a) at the peak in the magnetic age hardening curve – annealed for 3 hours, b) in the overaged condition – annealed for 8 hours.

Figures-21 to 23 show that the microstructures of the CR processed FePd alloys, which have been previously cold rolled to 97% reduction in thickness, consist of essentially entirely of equiaxed grains. These microstructures appear to have almost 100% CR transformed fraction. In the SEM studies significant fractions of material with the polytwinned morphology has not been detected for any of the three isotherms for the condition of peak coercivity and those associated with the decreasing coercivity at longer annealing times. During the magnetic hardening stage new  $L1_0$  ordered grains of FePd are seen to nucleate at heterogeneities in the deformed microstructure where large strain gradients exist, such as prior  $\gamma$ -phase grain boundaries, transition and / or micro-bands etc. The larger grains in the population of CR transformed fraction exhibit annealing twins. A significant fraction of grains are observed to be in the sub-micron size range. Average grain sizes have been determined for the conditions of maximum coercivity and in the overaged condition for all three isotherms using computer aided image analyses. Some pertinent results of this grain size distribution analysis have been summarized in table -3

These grain size measurements clearly indicate that a coarsening behavior is observed in the overaged state (table-3). Moreover, certain grains are seen to have grown to sizes very much larger than the average, producing extended large diameter tails in the grain size distributions. Microstructural observations of regions that exhibit some of these very large grains (figure-23b) show the presence of very small grains adjacent to the large grains. This local arrangement of grains of significantly disparate size may provide for conditions that could promote an abnormal mode of grain growth in the CR transformed fraction. Grain size distributions have been obtained for the peak coercivity and overaged conditions and a set of representative distributions are shown in figure-24a, 24b.

Table-3. Some pertinent grain size measurements for the condition of peak coercivity and in the overaged condition.

	<b>Treatment Temp.</b>	<b>Treatment Time (Min)</b>	<b>Coercivity Oe</b>	<b>Min grain size (Micron) Dmin</b>	<b>Max grain size (Micron) Dmax</b>	<b>Avg grain size (Micron) Davg</b>
1	400°C	10080	1389	0.035	0.901	0.234
	400°C	11520	1151	0.036	1.83	0.255
2	500°C	360	1251	0.05	2.18	0.407
	500°C	600	958	0.05	2.38	0.601
3	600°C	180	984	0.05	1.99	0.493
	600°C	480	705	0.08	6.36	1.13

The grain size distribution plots exhibit long tails at very large grain sizes. Thus, a small fraction of grains are seen to have grown rather rapidly and to much larger sizes than the average. Microstructural observations of such regions (fig-23b) show the presence of very small grains adjacent to these rather large grains. These local arrangements of disparately sized grains may be provide conditions that could promote an abnormal mode of grain growth in the CR transformed fraction.

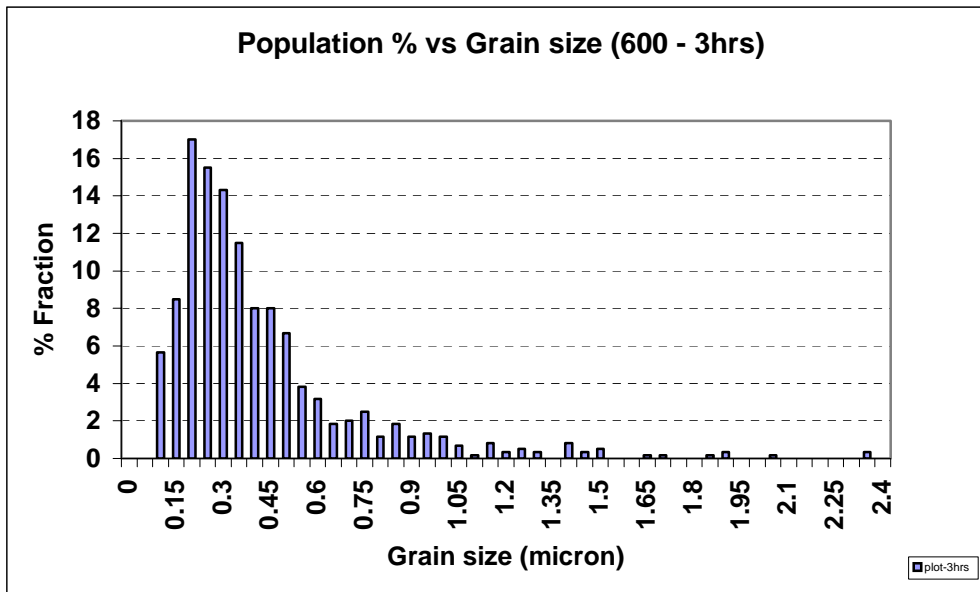


Figure-24a

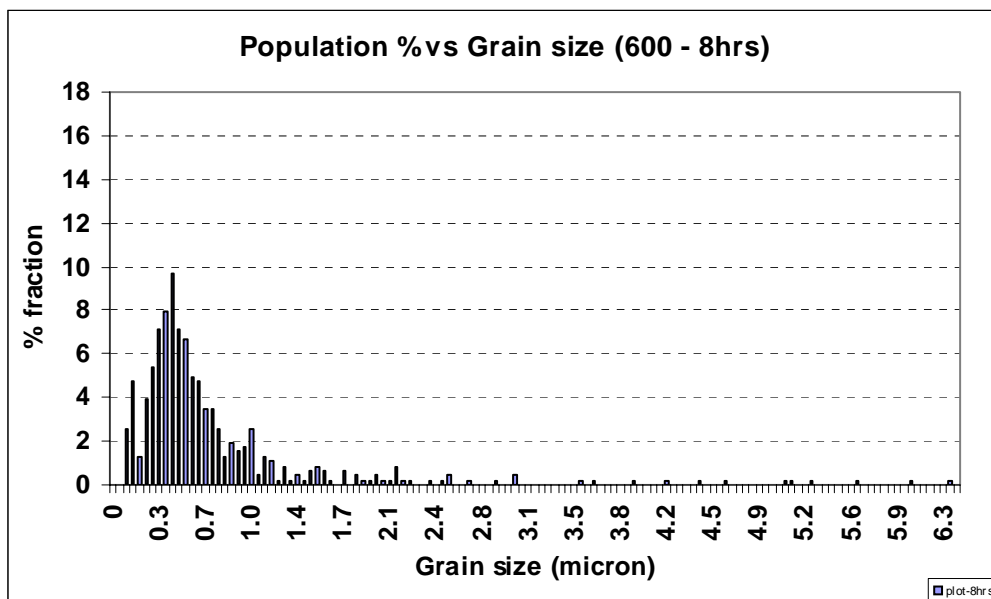


Figure-24b

Figure-24 Grain size distribution for samples order annealed at 600°C. a) For the peak coercivity condition, b) in the overaged condition.

To understand the local microstructural evolution, TEM investigations have been conducted on CR transformed samples in the peak and overaged condition. Representative TEM micrographs and selected area diffraction patterns (SADP) are shown in figures – 25.

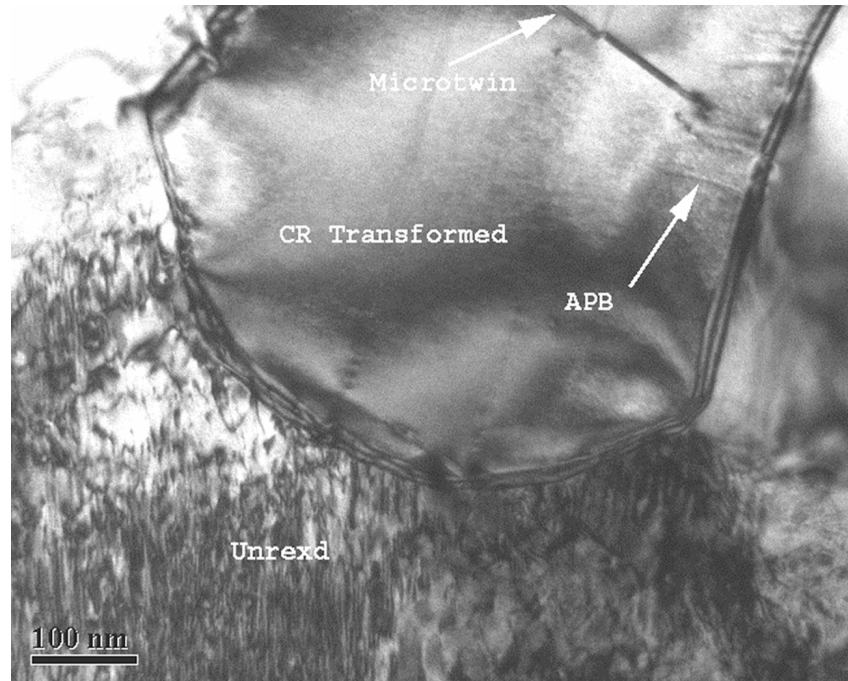


Figure-25a Bright field, multibeam TEM micrograph, near [001] ZA (3h-600C)

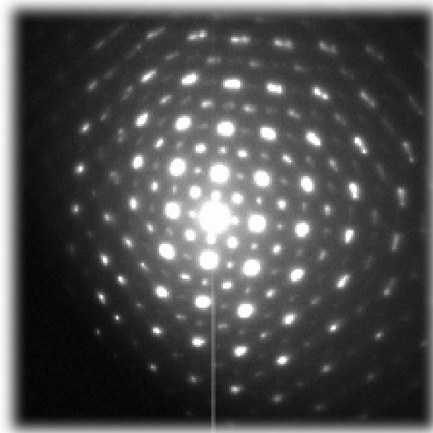


Figure-25b Selected area diffraction pattern, [001] ZA (3h-600°C)

As can be seen from TEM micrograph in fig-25a, microstructural details not observed in SEM investigations are revealed. Although SEM observations indicated an apparent 100% CR transformation, TEM reveals the presence of very minor fractions of non-CR transformed regions in the microstructure. The grain in the bottom part of fig-25a contains a high density of dislocations inherited from the deformed, disordered pre-annealing state and consists of  $\gamma_1$ -FePd variants formed by conventional nucleation and growth process. The selected area diffraction pattern obtained from this heavily defected region is shown in figure – 25b and it confirms the presence of the three possible orientation variants of the  $L1_0$  phase. The upper part of figure-25a shows a CR transformed grain of a single variant of  $\gamma_1$ -FePd, which contains some octahedral annealing twins and antiphase domain boundaries and exhibits very low dislocation content. These microstructural observations confirm the presence of a small volume fraction of non-CR transformed regions with a significant dislocation content in the microstructures associated with the maximum in magnetic coercivity for the cold rolled samples. However, it must be noted that these non-CR transformed fractions are observed to constitute less than 5% of the overall microstructure based on careful analyses of SEM and TEM data. This clearly supports the importance to conduct SEM and TEM studies in combination in order to obtain representative microstructural information related to the transformations studied here.

TEM observations have also been conducted for microstructures in the overaging or softening stage of the magnetic age hardening curve for 600°C isothermal annealing and are shown in figure-26.

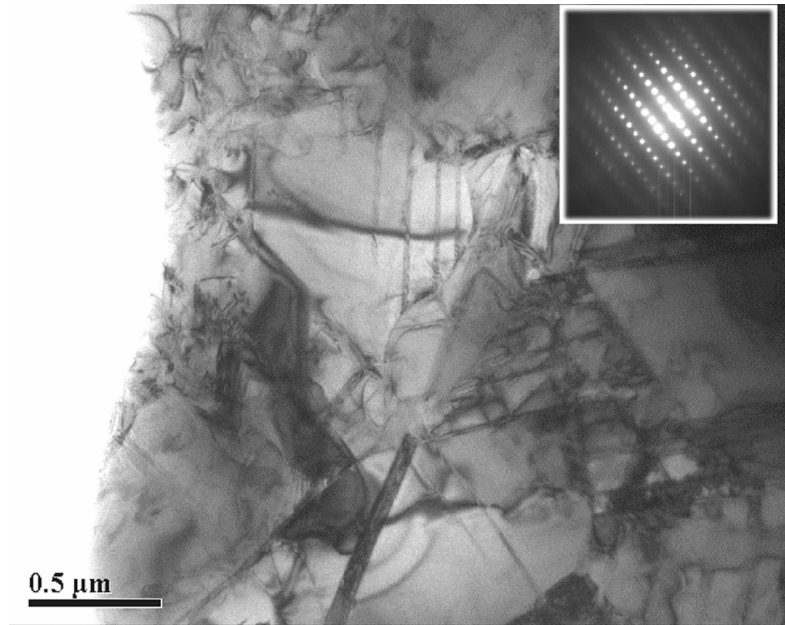


Figure-26a Bright field, multibeam TEM micrograph, near [001] ZA (8h-600C) and as inset a selected area diffraction pattern,[001] ZA, from a CR-transformed L10 FePd grain.

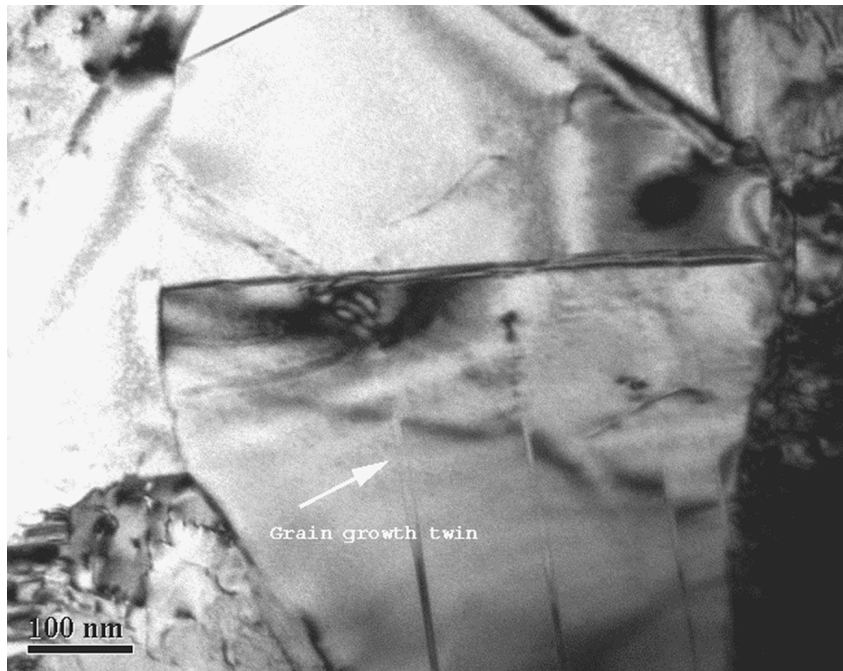


Figure-26b Bright field TEM micrograph of CR-transformed grains showing twinning (8h-600C)

The SADP inset in fig-26a confirms that this representative CR transformed grain is indeed of a single variant of  $L1_0$  ordered phase. As observed from the grain size data, these CR transformed grains are seen to increase in size during the softening stage. Grain growth twins are seen to emerge within these CR transformed grains and the number of grains that show such annealing twins is also seen to increase with increasing annealing time. Grain growth of CR transformed grains also appears to occur into the regions of the highly defected grains that have transformed by the conventional ordering process, as these highly defected regions are no longer seen to be present in the microstructure after a period of overaging.

#### **4.3.5 Discussion**

Microstructural evolution

The microstructural evolution in the cold rolled to 97% thickness reduction samples during order annealing can be analyzed over three regimes.

1. The microstructural evolution during the hardening stage of the magnetic age hardening curve.
2. The microstructural state corresponding to the maximum in coercivity.
3. The microstructural changes during the magnetic overaging, the softening stage.

Regarding 1.

During the hardening stage the microstructures consist of partially CR transformed regions and partially conventionally ordered regions (e.g. figure-20). It can be deduced from XRD investigations that the ordering process is not yet complete during the hardening stage. Moreover, the microstructure also reveals the presence of deformation content from the prior cold work in the conventionally ordering, non CR-transformed regions. Thus, under the

influence of both the driving forces (those for ordering and recrystallization) the combined reaction can continue to produce microstructural changes.

The ordering transformation in this CR process is facilitated by heterogeneous nucleation of new grains of  $L1_0$  phase at multiple locations in the microstructure. As observed previously for the single pass ECAP deformed samples, such nucleation events are favored at regions in the microstructure that can provide large amount of stored energy of cold work. Preferred locations for nucleation of new  $L1_0$  phase grains are greatly increased in the 97% cold deformed samples (figure-17) as compared to the single pass ECAP deformed material. Thus, there would be an enhanced probability for ordering via heterogeneous nucleation and subsequent growth of single variant, monolithic,  $L1_0$  grains in the microstructure for the 97% cold rolled material. This increased ability for transformation via the CR mode should be reflected in the microstructure in the form of an increased or majority fraction transforming via the CR mode. This hypothesis is indeed in agreement with the microstructural observations presented here.

Regarding 2.

XRD data showed that the ordering process is complete just about when the maximum in coercivity is attained. The microstructures in the completely ordered state are shown in figures – 21a, 22a, 23a and consist of nearly essentially 100% fraction transformed via the CR mode, leading to approximately equiaxed single variant  $L1_0$ -phase grains. A typical grain size distribution for the condition when ordering is complete is shown in figure – 24a. The nature of this grain size distribution is characteristic of a microstructural change that involves the simultaneous heterogeneous nucleation of new grains of the  $L1_0$  phase at multiple locations in the microstructure. Due to copious nucleation, at multiple number of sites the nucleated  $L1_0$  grains have relatively little chance to grow before they impinge as annealing progresses. This

argument can explain the relatively small (sub-micron) average grain sizes obtained in the fraction that has ordered via the CR mode. Thus, the microstructural observations and the grain size distribution data indicate that a heterogeneous nucleation process leading to essentially the entire microstructure transforming by the CR mode is responsible for the microstructural state achieved in the completely ordered state for the 97% cold deformed samples.

The FCC  $\rightarrow$  L1<sub>0</sub> ordering process in these intermetallics is a thermodynamic first order type phase transformation. A nucleation and growth model can be applied to this phase transformation. Due to interplay between the reducing driving force and an increasing mobility, with temperature approaching the equilibrium transition temperature ( $T_c$ ), the ordering reaction exhibits typical "C-curve" kinetics. The ordering kinetics are also a function of the prior deformation state. Accelerated ordering kinetics in the presence of

prior deformation have been reported previously [38,39]. A TTT curve for data from the literature [38] (for a prior deformation state of 90% cold deformation in wire drawing, an equivalent strain of  $\epsilon_{\text{equi}} > 3$ ) is shown in figure – 27. Superimposed on the literature based TTT curve are data points obtained from the experimental work conducted here.

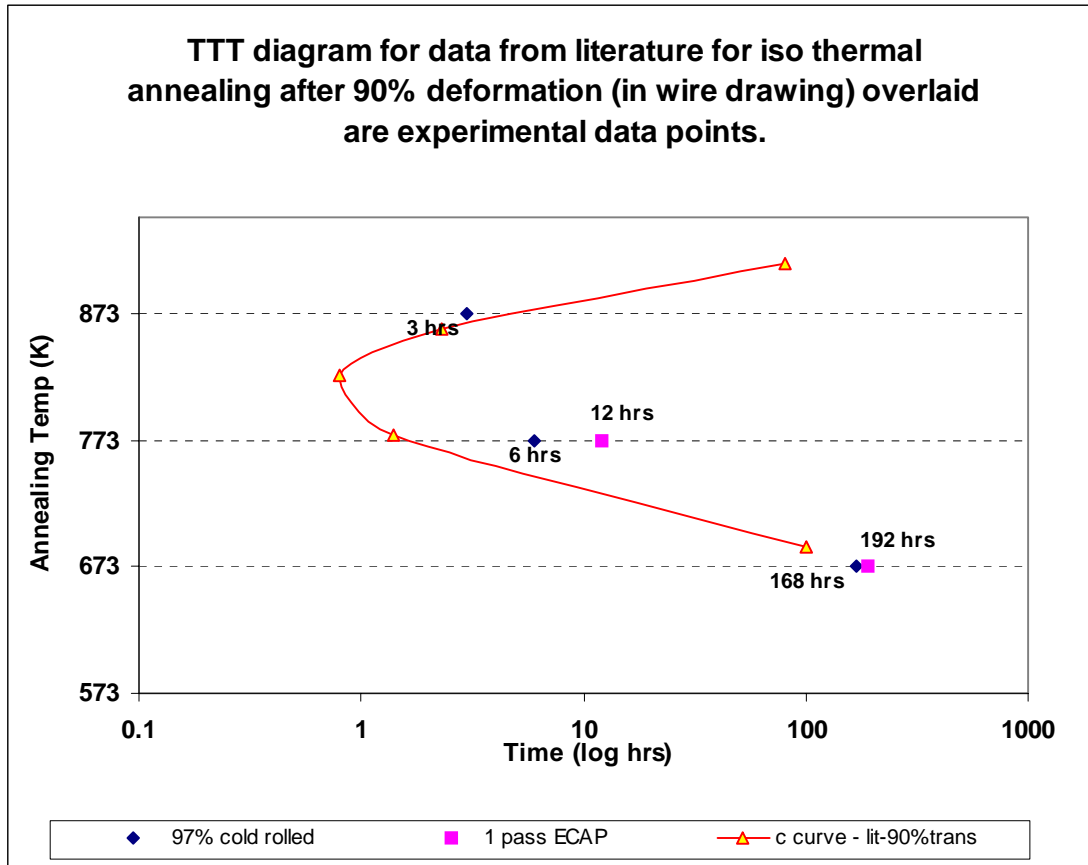


Figure-27 Comparison of previously reported [Greenberg] work on ordering kinetics with the experimental data obtained in this study.

The presence of prior strain of cold-deformation tends to alter the kinetics of the first order FCC  $\rightarrow$   $L1_0$  ordering phase transformation. Increasing prior strain of cold-deformation tends to shift the nose of the TTT curve (that represents the fastest rate of transformation) to higher temperature and to shorter time. Using the experimental data points obtained here for a slightly smaller effective strain than that imparted during wire drawing in the previously reported work it may be concluded that the nose of C-curve would be found at a temperature between 773 K and 883 K. In comparison with the data from the literature, the fastest transformation rate appears to be shifted to a slightly lower temperature and to a longer annealing time. Thus, given the smaller

amount of stored strain energy in the case of the samples studied here, the data obtained in this experimental study is in good qualitative agreement with these previous studies [38,39].

Following a particular isotherm in figure-27, e.g 773 K, the fastest kinetics of transformation can be observed for the condition with the higher strain of prior deformation (90% - wire drawn). These observations can be rationalized based on the kinetics of the process. The activation energy barrier for ordering transformation in the CR mode is reduced due to contributions from an additional driving force  $\Delta G_d$  (equ-5). With increasing prior strain of deformation a smaller activation energy barrier for ordering transformation would be present, and therefore the kinetics of the process would be enhanced. The prior strain of deformation would also affect the ordering process in the conventional mode; however its influence on the conventional ordering mode does not appear to be strong.

The average grain size in the completely ordered state is larger for transformation at high temperature (493 nm at 600°C) than at intermediate temperature (407nm at 500°C) or low temperature (234nm at 400°C). The ordering transformation in the CR mode is a nucleation and growth process. At 600°C due to faster diffusion kinetics the growth process is dominant. Once nucleated the grains are able to grow at much faster rate, therefore leading to a larger average grain size in the completely ordered state. At a lower temperature of 400°C, the process is nucleation dominated. Due to slower diffusion kinetics the nucleated grains have a small chance to grow, thus leading to a smaller average grain size.

An investigation of the microstructure using TEM reveals microstructural details not observed in SEM. Based on SEM analyses, at the completion of ordering process, it was deduced that the microstructure in entirety consisted of regions transformed via a CR mode. However TEM studies showed that after annealing at 600°C for three hours, there are certain regions in the

microstructure that have ordered and still have prior deformation content present (figure-24a, b). The presence of these apparently non CR transformed regions can be explained based on a kinetic argument. The dislocation density present in the microstructure is not uniform. The deformed microstructure consists of a dislocation substructure with cell walls (high dislocation density) and cell interiors (low dislocation density). In the cell interiors with lower dislocation density the kinetics for ordering by the conventional mode and by the CR mode may become comparable. Thus, in these regions the conventional ordering mode may prevail producing all three variants of the  $L1_0$  phase.

Regarding 3.

Microstructural observations and grain size measurements have been performed in the overaged condition. In comparison with the maximum coercivity condition, for the overaged condition the peak in grain size distribution shifted towards larger grain sizes. Furthermore, the fraction of the population of grains in the larger size bins increased. Based on the grain size distribution data and microstructural observations it can be inferred that grain growth occurred during the microstructural evolution in the overaging part of the magnetic age hardening curve. The grain size distribution in the overaged state depicts a very long tail (figure-23b). Grain sizes as large as 6  $\mu\text{m}$  have been measured in these overaged conditions. Figure-24b also shows the presence of very small grains adjacent to these large grains. Such observations may indicate conditions suitable to promote abnormal grain growth in certain regions of the microstructure for the overaged condition. However, the data obtained here is not sufficient to warrant any general conclusions regarding distinction between normal or abnormal mode of grain growth.

TEM observations (figure-26a, 26b) in the overaged condition reveal the absence of any deformation content from the prior cold working. Since the material is in the completely ordered

state at the start of the overaging process, the microstructural change does not involve a transformation and can be treated purely as an annealing phenomenon. During overaging, the moving grain boundaries are able to sweep the dislocation and other defect content from the grains that are consumed. Thus it can be concluded that the microstructure in the overaged state consists of equiaxed coarsened grains that contain certain density of annealing twins.

Magnetic Property evolution –

The maximum value of coercivity observed after CR processing (1389 Oe) represents an approximately five fold increase with respect to the values typically obtained for equiatomic FePd with the polytwinned microstructure (~250 Oe). Thus, CR processing is suitable to enhance hard magnetic properties in equiatomic FePd.

Magnetic age hardening behavior, consistent with previous observations [5,38,40,41] is observed here for samples that have been annealed after 97% thickness reduction by cold rolling. The evolution of coercivity,  $H_c$ , with annealing time for each of the isotherms shows three characteristic regions as depicted in figure 18:

Region 1 - Increasing coercivity with increasing annealing time (Hardening stage); Region 2 - Attaining of the coercivity peak (Peak coercivity); Region 3 - Decreasing coercivity (magnetic overaging) for further increased annealing times (Softening stage).

Moreover, figure-18 indicates that this characteristic ‘magnetic age hardening’ behavior is observed for all the various processing conditions explored here. However, some important differences pertain with respect to the different processing conditions. For instance, the rate of approach to the peak coercivity and the maximum value of coercivity obtained for a given amount of prior strain of deformation depend on the annealing temperature. Thus, by using various processing temperatures at a fixed amount of strain the temperature-time space of

processing parameters has been probed. For instance, for the cold rolled FePd the maximum in coercivity is observed the earliest (3hrs) at an annealing temperature of 600°C, whereas nearly 7 days are required to achieve a maximum in coercivity at 400°C. The XRD studies for these CR processed samples after 97% cold deformation by rolling have confirmed the attainment of a fully ordered structure with the equilibrium LRO-parameter after annealing times corresponding to those required for achievement of a maximum in coercivity. Thus, the monotonic increase in the coercivity in all these CR processed samples during the hardening stage (Region 1) can be attributed to an increase in the volume fraction of ordered phase, which is reflected in the evolution of the long range order parameter (LRO). This is identical with the conclusions drawn from the studies of the ECAP-deformed samples (section 4.2.2). The rate of increase in the LRO is linked with the kinetics of the CR process of ordering and the evolution of microstructure as ordering progresses. The faster diffusion rates due to the high atomic mobility at 600°C lead to a much more rapid attainment of a completely ordered state leading to a maximum in coercivity after 3 hours. The much slower diffusion rates and reduced atomic mobility at the lower annealing temperature of 400°C leads to maximum coercivity after 7 days (168 hours, almost 60 times longer than at 600°C) for the essentially completely CR transformed microstructure.

The coercivity,  $H_c$ , describes the value of external magnetic field strength required to fully demagnetize ( $M=0$ ) the sample after saturation ( $M= M_{\max} = M_s$ ). The value of the coercive force,  $H_c$ , depends on phenomenon associated with the interactions of magnetic domain walls with microstructural entities, such as grain boundaries and other crystal defects. Thus, the maximum in coercivity obtained after annealing for a given  $\epsilon_{cw}$ , depends upon the grain size, the distribution and nature of planar defects in the CR transformed fraction, as well as the microstructural morphology. The effects of microstructure on coercivity have been previously

studied [8,41,42,43] and two different principal coercivity enhancement mechanisms have been proposed. The first mechanism is based on the nucleation of a reversed magnetic domain during magnetization reversal. It is analogous to the ‘heterogeneous nucleation’ theory from phase transformation treatments and takes into account the relative ease with which the nucleation and growth of reversed domains can occur. The coercivity enhancement predicted by this nucleation type mechanism is inversely proportional to the grain size and can be expressed as follows [43]

$$H_c = \beta (\gamma / M_s) (1/D) \quad \text{--} \quad (6)$$

Here  $\beta$  is a geometrical factor related to the details of nucleus geometry of the reversed magnetization domain,  $\gamma$  is the magnetic domain wall energy (17 ergs/cm<sup>2</sup>),  $M_s$  is the saturation magnetization (1100 emu/cm<sup>3</sup>) and  $D$  is the grain diameter.

Microstructural entities can also interact with moving domain boundaries and act as pinning centers or obstacles to these moving boundaries. A second coercivity mechanism based on a pinning effect associated with microstructural entities retarding moving magnetic domain boundaries has also been discussed previously [43,44]. The coercivity enhancement due to planar defects, such as grain boundaries, that have a width  $r_0$  much smaller than the magnetic domain wall width ( $\delta$ ) can be expressed by the pinning mechanism as –

$$H_c = \alpha (2K_1/M_s) - N_{\text{eff}} M_s \quad \text{--} \quad (7)$$

Here

$$\alpha = (1/5.19) (\pi r_0 / \delta) [(A/A') - (K/K')] \quad \text{--} \quad (8)$$

In the above equations 7 and 8,  $A'$ ,  $K'$  and  $A$ ,  $K$  are constants describing the atomic exchange coupling and magnetocrystalline anisotropy of the obstacle and the matrix containing the magnetic domain wall.  $N_{\text{eff}}$  is an effective demagnetizing factor. The factor  $\alpha$  would also be a function of a statistical factor that accounts for the number of interactions that might occur

between a moving domain boundary and a pinning entity per unit of domain wall. An increased number of interactions would produce a larger value for  $\alpha$ .

Considering the effect of grain size on the value of the peak or maximum in coercivity obtained for the different isothermal annealing conditions after 97% cold deformation can be based on equation-6 implies an inverse relation between coercivity and grain size. Thus, if a nucleation type coercivity mechanism is responsible for the peak coercivity observed here during annealing of the fully CR transformed cold rolled FePd the microstructure with the smallest grain size should exhibit the highest coercivity. Furthermore, for an increasing grain size in the essentially equiaxed microstructures of the fully ordered FePd a reduction in coercivity would be expected. These two correlations between grain size and coercivity are indeed observed here. Hence, it is tempting to conclude that the large coercivity observed in the CR transformed FePd originates via a nucleation type coercivity mechanism. However, it must also be noted that the increase in grain size during the overaging or softening stage occurs by grain growth and is facilitated by motion of mobile grain boundaries, presumably high-angle grain boundaries. The mobile grain boundaries sweep-out the defect content of the grains that are consumed (see previous section). Thus, grain growth naturally reduces the density of planar obstacles for magnetic domain wall motion, such as grain boundaries and APB's in the coarsening microstructure. Hence, the frequency of interactions between moving domain walls and pinning grain boundaries would decrease, lowering the contributions to coercivity from a pinning type mechanism too (equations 7, 8). Conversely, a denser obstacle field is present in the smaller grain size microstructures and thus the statistical factor for interactions of the moving domain wall with obstacles would increase and according to equations 7, 8 the coercivity would increase. Therefore, contributions to coercivity enhancement from a pinning type mechanism would also be expected to increase

for microstructures with reduced grain size. The microstructural observations and coercivity measurements are in good qualitative agreement with these theoretical considerations. Maximum coercivity (1389 Oe) is indeed observed for a microstructure with the smallest average grain size (234nm) in the CR transformed ordered microstructure. Also the smallest enhancement (984 Oe) is observed for a condition (600°C-3hours) that produces the largest average grain size (493 nm) for the essentially fully equiaxed microstructures. Intermediate peak coercivity enhancements are obtained for other processing conditions that produce intermediate average grain sizes in the morphologically equiaxed microstructures produced by the CR mode of the ordering transformation.

As can be seen from the data in table-3 increasing the annealing time past the maximum in the magnetic age hardening curve leads to grain coarsening in the equiaxed microstructures. Based on the previously discussed nucleation and pinning models for coercivity enhancement, it can be expected that an increasing grain size should lower the magnetic coercivity. The experimental observations agree well with this prediction based on equation 7. In fact, figure-18 and table-3 show a decreased coercivity for a microstructural state associated with a coarsening grain structure.

The effect of microstructure on magnetic coercivity also becomes evident if the maximum in coercivity attained after single pass ECAP and annealing at 500°C is compared with the 97% cold deformed and annealed at 500°C condition. In the latter case, which represents a much larger amount of strain of cold work, the coercivity is almost twice as large as for the former. A comparison of the microstructures (figure-13a and figure-22a) reveals the varying proportions (about 36% and >95%) of the microstructures that have CR transformed to equiaxed, nearly stress free, ordered  $L1_0$  grains. A larger proportion of the microstructure in the single pass ECAP

sample has ordered via the conventional mode of nucleation and growth of coherent  $L1_0$  phase precipitates. The smaller volume fraction of CR transformed grains in the ECAP sample can be expected to lead to a reduced pinning contribution from grain boundaries to the coercivity. The polytwinned morphology is virtually absent in the sample that has been CR transformed after 97% cold deformation. Moreover, the average grain size in these latter samples is also of much smaller scale than the average grain size in the CR transformed fraction in the ECAP and annealed sample. These factors would therefore lead to an enhanced contribution from the nucleation and also from the pinning mechanisms to coercivity in the 97% cold deformed and annealed samples as compared to the single pass ECAP and annealed samples.

## 5.0 SUMMARY AND CONCLUSIONS

The coercivity of the equiatomic FePd alloys depends upon their microstructure. Microstructural morphologies such as the polytwinned structure have a detrimental effect on the hard magnet properties of these alloys. A microstructural state comprising of equiaxed, monolithic, single variant  $L1_0$  grains is found to be conducive to the enhancement of coercivity. In this study thermomechanical processing strategies involving a combined reaction of recrystallization and  $FCC \rightarrow L1_0$  phase transformation have been employed to alter the microstructural state of the equiatomic FePd alloy. Both the scale and the morphology of the microstructures have been altered using the combined reaction processing routes. The microstructure and coercivity evolution is found to depend on the processing parameters, namely the prior strain of deformation, the annealing temperature and the time of annealing. Hence, a matrix of these parameters has been explored in attempts to optimize the microstructure and to obtain enhanced coercivity. Two techniques have been employed to impart different amounts of strain of deformation. A low strain of deformation ( $\epsilon_{cw} = 0.6$ ) has been imparted via equal channel angular pressing (ECAP). The effect of other parameters (temperature and time) on the evolution of microstructure and coercivity in these samples has been studied. In contrast a higher, prior strain of deformation ( $\epsilon_{cw} = 3.0$ ) has been imparted using cold rolling to 97% reduction in thickness. The effect of temperature and time on microstructure and coercivity evolution in these samples

has also been studied. A comparison between the results obtained after these different processing conditions has yielded the following main conclusions:

1. The highest coercivity (1389 Oe) is obtained for the microstructure that has the smallest average grain size in the completely ordered state (234nm) and approximately 95% fraction of the microstructure consisting of equiaxed, monolithic  $L1_0$  phase grains. This microstructural state is obtained in the 97% cold rolled state after 7 days of order annealing at 400°C.
2. The rate of the ordering transformation is enhanced in the presence of stored strain energy from prior deformation. The samples that exhibit a higher amount of stored strain energy from prior cold deformation show larger enhancement in the ordering kinetics.
3. The mode of the ordering transformation depends on the prior strain of deformation. A higher amount of prior strain of deformation increasingly favors a combined reaction (CR) mode of ordering over the conventional mode of ordering.
4. The microstructural evolution is a function of the mode of transformation. A higher prior strain of deformation (about 3.0 for 97% cold rolling) leads to nearly 100% fraction transformation via the CR mode, with average grain sizes in the transformed fraction ranging from 234 nm to 493 nm. The lower prior strain of deformation (about 0.6 for one pass ECAP) allows for the CR mode and conventional mode to simultaneously achieve the ordering transformation. A smaller fraction of the microstructure in the completely ordered state (e.g. 36% after 12 hours at 500°C) consists of the equiaxed, monolithic grains of  $L1_0$  phase formed via the CR mode. Hence, for some critical amount of stored strain energy from prior cold deformation, which is larger than that accomplished by imparting an equivalent strain of about 0.6 at room temperature, the kinetics of the

combined reaction mode of ordering are sufficiently rapid to transform the entire sample volume.

5. Grain coarsening is observed in the microstructures during overaging. The grain size distributions hint at the presence of an abnormal mode of grain growth occurring in some of these coarsening microstructure.
6. The peak in the magnetic age hardening curve is achieved when the ordering transformation is complete.
7. Qualitatively it has been established that the value of the coercivity obtained at the peak in the magnetic age hardening curve is a function of the fraction transformed via the CR mode and grain size in the CR transformed fraction.
8. The grain growth process can be qualitatively linked to the decrease in coercivity during the overaging part of the magnetic age hardening curve.

## 6.0 RECOMMENDATIONS FOR FUTURE WORK

1. Increased Prior Strain of Deformation - In this experimental work it has been established that the CR mode of ordering transformation can become dominant with an increased prior strain of deformation. Moreover it has also been established that the ordering transformation in the CR mode occurs via heterogeneous nucleation of single variant  $L1_0$  phase grains. This heterogeneous nucleation process is favored at sites in the microstructure with large deformation content. It has also been qualitatively established that the relatively small grain size in the CR transformed fraction is responsible for the enhanced coercivity in these microstructure. Thus by increasing the amount of prior strain of deformation to even larger values than those used in this study ( $\epsilon_{cw} > 3.0$ ), nucleation could be made favorable at an increased number of sites in the microstructure. The ordering transformation could be made nucleation dominated. Thus order annealing treatments of these severely plastically deformed samples could lead to microstructures that have average grain sizes in the truly nanoscale regime and would be expected to exhibit enhanced coercivities.

2. Quantitative Coercivity Mechanism Analysis - A qualitative relation between the average grain size and the coercivity has been established in this study. A rigorous quantitative coercivity mechanism analysis would require the measurement of such additional parameters such as the average density of various defects such as APBs, annealing twins etc. in the microstructure, the orientations of different grains in the microstructure. Moreover better understandings of the

interactions of various microstructural entities with moving domain walls would also have to be developed for the Fe-Pd system.

## BIBLIOGRAPHY

1. Weller,D., and Moser,A. (1999), IEEE Trans. Magn. **35**, 4423.
2. Magat,L.M, Yermolenko,A.S., Ivanova,G.V., Makarova, G.M., and Shur,Y.A.S. (1968) Fiz. Metal. Metalloved. **26**, 511.
3. Zhang,B., Lelovic,M., and Soffa W.A (1991). Scripta met. mat. **25**,1577.
4. Vlasova,N.I., Kandaurova, G.S., Shchegoleva, N.N., (2000). J Magn. Magn. Mater. 222,138.
5. Klemmer,T.,J., (1995) PhD thesis, University of Pittsburgh.
6. Khachatryan,A.G. (1983) In: ‘Theory of Structural Transformations in Solids’,p368, John Wiley & Sons, New York.
7. Yanar, C., Wiezorek, J.M.K., and Soffa, W.,A.(2000) In: Phase Transformations and Evolution of Microstructure in Materials, p39-54, edited by-Turchi, P.et al. TMS Warrendale.
8. Klemmer,T., Hoydick,D., Okumura,H., Zhang,B., Soffa., W.A., (1995) Scripta Metall Mater **33**,1793.
9. Rao,M., (1997) PhD thesis, University of Pittsburgh.
10. Hirsch, J., Lucke, K., Hatherly,M., (1988) Acta Met., **36**, 2905.
11. Hirsch, J., Lucke, K., (1988) Acta Met., **36**, 2863.
12. Duggan,B.,J., Sindel,M., Kohlhoff, G.D., and Lucke, K (1990) Acta Met., **38**, 103.
13. Reed-Hill, R. E., and Abbaschian,R.,(1992) In :Physical Metallurgy Principles, p247, PWS Pub. Co. Boston.
14. Westbrook, J.H. (1977) In: Intermetallic compounds, p398, Robert E. Krieger Pub. Co. NY.
15. Cahn,R.,W., (1996) In: Physical metallurgy **vol-3**, p2427, edited by - Cahn,R.,W., and Haasen., P. North Holland Pub.Co.NY.

16. Ferran,G.L., Doherty, R.D., Cahn,R.W. (1971) *Acta Metall.***19**,1019.
17. Faivre,P., Doherty,R.D (1979), *J Mater. Sci.* **14**, 897.
18. Ray,R.K, Hutchinson,B.W., Duggan,B.J. (1975), *Acta Metall.* **23**,83.
19. Ray,R.K., Jonas,J.J., Hook, R.E (1994), *Internat. Mater. Rev.* **39**,129.
20. Doherty,R.D., (1974), *Metal Science* **8**,132.
21. Cahn R.W., (1950) *Proc. Phys. Soc.* **A63**,323
22. Hu ,H. (1962) *Acta Metall.***10**,112.
23. Beck, P.A., Sperry, P.R., (1950) *J Appl. Phys.* **21**,150.
24. Hutchinson,W.B., Nes,E. (1992), *Mater. Sci. Forum* **94-96**,385.
25. Vandermeer,R.A., (1995) in: 16<sup>th</sup> RisØ symp., p 193. eds.N.Hansen et al.
26. Hornbogen, E., (1979) *Met. Trans.* **10(A)**, 947.
27. Hornbogen, E., ‘Phase transformations 87’, in *Phase transformations’87*, eds Lorimer G.W. (1987) *Inst. of Metals: Univ. of Cambridge.* p394.
28. Dieter,G.E., (1998) In: ‘Mechanical Metallurgy’
29. Luis Perez, C. J., (2004) *Scripta Mat.* **50**, 387.
30. Tetsuo, A., (2001) *Scripta Mat.* **44**,575.
31. Engqvist, H., Uhrenius,B., (2003) *Intl. J. of Refractory metals and hard materials.* **21**, issue 1-2, 31
32. Cullity,B.D. (1972) In: *Introduction to magnetic materials*, p312, Addison Wesley Pub. Co. Reading, Mass.
33. Klemmer,T.J., Soffa W.A., (1994) In: *Solid-Solid Phase transformations*, p969, edited by Johnson,W.C., Howe, J.M., Laughlin,D.E., Soffa,W.A., TMS Warrendale.
34. Berger,A., Willbrandt,P. J., Ernst,F., Klement,U., and Haasen,P. (1988) *Prog. Mat Sci.* **21**,1
35. Willbrandt,P.J., Haasen,P., (1980) *Z. Metallkde* **71**, 273.
36. Doherty,R.D., Hughes,D.A., Humphreys,F.J., Jonas,J.J., Jensen,D.J., Kassner,M.E., King,W.E., McNelly,T.R., McQueen, H.J., and Rollet, A.D. (1997) *Mat Sci.Eng.* **A238**, 219.

37. Poter,E. Easterling,W. (2001) In: ‘Phase transformations in metals and alloys’ , p305,
38. Greenberg,B.A.,Volkov,A.Yu., Kruglikov,N.A., Rodionova,L.A., Grokhovskaya,L.G., Guschin G.M., Sakhanskaya, I.N. (2001) The physics of metals and metallography, **92** vol-2,167.
39. Gushchin,G.M., Berseneva, F.N., (1987), Fiz Metal. Metalloved., **63**, vol-5, 926.
40. Teytel,Ye.I, Gushchin,G.M., (1988) Phys. Met. Metall. **65**, vol-2,114.
41. Ristau,R.A., Barmak,K., Lewis,L.H., Coffey,K.R., Howard,J.K., (1999), J. Appl. Phys, **86**,4527.
42. Kronmuller,H., Fahnle,M.,(2003) In: Micromagnetism and the microstructure of ferromagnetic solids.p90, Cambridge University Press.
43. Kronmuller,H., Durst, K.D., Sagawa, M. (1988) J. Magn Magn Mater.**74**, 291.
44. Kronmuller,H., (1991) In: Micromagnetic Background of hard magnetic materials, Supermagnets, hard magnetic materials.p461, edited by – Long,G.J., Grandjean,F., Kluwer Academic publishers.